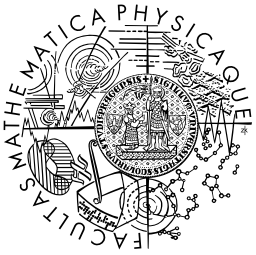

FACULTY
OF MATHEMATICS
AND PHYSICS
Charles University

MASTER THESIS

Bc. Jakub Jambrich

Consistent non-equilibrium thermodynamic modeling of hydrogen fuel cells

Mathematical Institute of Charles University

Supervisor of the master thesis: RNDr. Michal Pavelka, Ph.D.

Study programme: Mathematical and Computational Modelling in Physics

Prague 2022

I declare that I carried out this master thesis independently, and only with the cited sources, literature and other professional sources. It has not been used to obtain another or the same degree.

I understand that my work relates to the rights and obligations under the Act No. 121/2000 Sb., the Copyright Act, as amended, in particular the fact that the Charles University has the right to conclude a license agreement on the use of this work as a school work pursuant to Section 60 subsection 1 of the Copyright Act.

In ..... date ....

Author's signature

Before the beginning of my Master's thesis, I want to express gratitude to all people helping me with the work on my Master's thesis and during my studies.

First, I want to thank Professor Jay Benziger for his data, as it would be impossible to do this thesis without them.

Further, I want to thank Tomáš Němec for helping me interpret some first model results, which seemed illogical to my supervisor and me.

I also want to thank my consultant Ondřej Kincl, for helping me with the code while I got used to Julia language syntax and the weird sign conventions inside the VoronoiFVM library.

The biggest gratitude belongs to my thesis supervisor Michal Pavelka, for the plenty of hours that we spent discussing many problems. For his dedication to standing in front of the whiteboard with me until we reached the solution. Also, for his quick responses to my emails, even during the weekends, holidays, and nights, which really are not standard nowadays.

Finally, I have to thank my girlfriend Sára. I could write down for what, but she knows the list maybe even better than me.

Title: Consistent non-equilibrium thermodynamic modeling of hydrogen fuel cells

Author: Bc. Jakub Jambrich

Institute: Mathematical Institute of Charles University

Supervisor: RNDr. Michal Pavelka, Ph.D., Mathematical Institute of Charles University

Abstract: At first, a classical irreversible thermodynamic model of the hydrogen pump is derived in this thesis. The model is then numerically implemented by using the Finite volume method in the *VoronoiFVM* library in Julia. The numerical implementation is further used to explain the measured experimental data from [1]. The plateau observed in the Voltage-current figure could not be explained in the original work, as the membrane was approximated with a single point. Such a zero-dimensional model did not predict the plateau, and it was believed to originate from some Interfacial effects. This work will focus on the correct implementation of the equations inside the membrane and try to explain the observed effects using no additional assumptions.

Keywords: Non-equilibrium thermodynamics fuel cells numerics

Contents

Introduction

In a world where humanity will be running out of oil, gas, and coal in 35, 37, and 107 years respectively (predictions from [2]), the reduction of energy consumption and more effective energy management is needed. However, the limited amount of fossil fuels is not the only primary issue. By the time humanity runs out of fossil fuels, our environment will be irreversibly damaged if the greenhouse gas emissions will not be dramatically reduced ([3]). As renewable energy sources like solar or wind energy are not even able to produce a steady amount of electricity, not to mention producing the electricity as much as needed at the moment. Therefore, an effective way of storing energy must be found ([4]).

Together with batteries, the fuel cells can play an essential role in future energy storage. Whereas batteries are costly to store huge amounts of energy (for example, from solar power plants in summer for usage during winter), they can release huge amounts of energy quickly, which is needed sometimes to cover the peaks in the energy supply system. On the other hand, fuel cells are much cheaper for storing large portions of energy, but their output power is more limited. To make use of the advantages of both systems and eliminate their disadvantages, the system which combines batteries and fuel cells can be used as proposed in the article [5].

Another usage of fuel cells, which is already in use nowadays, are fuel cells as a source of power for cars (instead of diesel or petrol engines). It is important to point out that besides the fuel cell, each such car also has a small battery, which is used when the car needs more power than the fuel cell can deliver for a short period of time (for instance, while accelerating rapidly). That is the same principle as the one for storing energy presented in the previous paragraph. The current models of electric cars use the PEM fuel cell with carbon electrodes with platinum particles, where the platinum particles are reaction sites as platinum is an excellent catalyst for HOR reaction [6]. Much effort is nowadays concentrated on reducing the amount of platinum needed for a fuel cell with specific output power, as platinum is costly.

Although the effort to reduce the amount of platinum is crucial from a commercial point of view ([7]), understanding another process inside the PEM fuel cell also needs to be studied. So far, the mechanism of transport of H^+ ions and water through the proton exchange membrane is not fully understood. As the transport equations are complex, numerical simulations are used to solve them. Moreover, while the fuel cell is operating, the flow of the fuel, air, and water are tough to predict and make the models very complex and full of unknown parameters. This makes verifying the theories very complicated. If our intention is only to study the processes inside the membrane, the fuel cell is an unnecessarily complicated experimental setup.

Therefore, for investigating the transport processes inside the membrane with better accuracy, the simple experimental setup, which consists of a PEM membrane sandwiched between two electrodes with hydrogen on both sides, was constructed by the team of J. Benziger [8]. The setup can operate in a stationary state (where species concentrations and partial pressures on both electrodes surfaces can be considered constant spatially and in time), making the whole analysis

much easier. The goal of this thesis is to explain the data measured on the setup and published in [1] using a more sophisticated theoretical model than in the mentioned article. Thanks to the construction of the experiment, the system is big enough (with respect to the membrane width) that it can be considered to be homogeneous in all the directions in the plane, parallel to the membrane. Therefore, it is sufficient to consider a one-dimensional model (the only relevant dimension is the one perpendicular to the surface of the membrane) with a constant temperature.

The goal of the thesis is to make a one-dimensional model of a hydrogen pump. After that, we will aim to find the unknown parameters of the model to explain the measurements from [1]. Than, we will try to use the model to explain why are there problems with the measurements of drag coefficient - which expres how the proton flux affects the water flux and vice versa. We will also provide a better way how to determine the drag coefficient experimentally.

1. Theory

1.1 Classical Irreversible Thermodynamics

In contrast to equilibrium thermodynamics, Classical Irreversible Thermodynamics (CIT) is its extension to more realistic situations, where inhomogeneities and respective flows have to be taken into account. The typical examples described earlier as separate theories by Fourier (1822), and Fick (1855) are heat conduction (where inhomogeneity in temperature occurs and results in respective heat flux) and diffusion (where inhomogeneity of concentration occurs and results in respective diffusion flux). CIT theory aims to formulate a theory of thermodynamics near the equilibrium and derive a procedure for compiling thermodynamic equations in the field of its validity [9].

1.1.1 Local equilibrium

In CIT, we consider the studied body not to be in thermodynamical equilibrium. However, in equilibrium thermodynamics, we have defined all the thermodynamical quantities, such as temperature, entropy, chemical potential, etc., only in the thermodynamical equilibrium. To make it possible to define them properly for some body, which is not in equilibrium, we have to introduce the concept of *local equilibrium*.

To do so, we need to divide the body into a system of cells. Each cell is small enough to be in equilibrium, but on the other hand, big enough that fluctuations caused by the kinetics of molecules inside the cell are negligible within the thermodynamic limit. The size of such cells is subject to further discussion and can be found in [10]. A *local equilibrium hypothesis* states that once equilibrium is achieved in all cells at a given instant of time. However, they are not equilibrated with each other. This leads to mass and energy exchange between neighboring cells. The speed of exchange with respect to the time scale of equilibration inside a cell is expressed with a quantity called Deborah number.

Suppose we denote by the τ_m equilibration time inside one cell and by the τ_M macroscopic equilibration time, which magnitude corresponds to the time scale on which the studied process takes place. In that case we define the Deborah number as $De = \tau_m/\tau_M$. For $De << 1$ local equilibrium hypothesis is fulfilled with reasonable accuracy, as the time scale on which studied processes take place is much longer than τ_m, which means that studied variables stay unchanged over the time τ_m. The main consequence of the local equilibrium theorem is that thermodynamic state variables, well-defined locally, can be defined outside of equilibrium as continuous functions of time.

Now we can write Gibbs equation for entropy density s (in this chapter, we define density not per unit of volume as usual but per unit of mass) of N-component fluid as ([10])

$$ds = \frac{1}{T}du + \frac{p}{T}dv - \frac{1}{T}\sum_{i=1}^{N}\mu_i dc_i \tag{1.1}$$

where u is a density of internal energy, v is the density of volume, which is $v = V/M = 1/\rho$ where ρ is standard density in kg/m^{-3}, c_i is the mass fraction

of i-th component of the mixture, μ_i is the chemical potential of the respective component and T and p are absolute temperature and pressure respectively.

Analogically, we can derive a more general equation for an arbitrary set of N extensive state variables A_i (and respective densities a_i) and corresponding conjugate intensive state variables α_i as

$$ds = \sum_{i=1}^{N} \alpha_i da_i. \tag{1.2}$$

From [10] we can assume that after taking the lagrangian time derivative [1] of expression 1.2, it will remain in shape

$$\frac{ds}{dt} = \sum_{i=1}^{N} \alpha_i \frac{da_i}{dt}. \tag{1.3}$$

1.1.2 Balance of the entropy

Let's consider some body, which is not equilibrated (neither with the environment nor by itself) and has o volume V, surface Σ and at some tome t has entropy S. Then we can distinguish two ways of entropy change ([10])

$$\frac{dS}{dt} = \frac{d^i S}{dt} + \frac{d^e S}{dt}. \tag{1.4}$$

First, is entropy produced inside the body $d^i S/dt$ and second is entropy exchanged with its surroundings $d^e S/dt$. At this point, it is important to note that the first term in 1.4 always has to be non-negative (this can be viewed as the second law of thermodynamics generalized for non-equilibrium thermodynamics). The second can be both positive and negative (for example, when the air conditioner is turned on in a closed room, its entropy decreases due to the negativity of the second term).

Next we introduce new quantities called entropy flux $\mathbf{J_s}$ and entropy production σ_s. Which can be defined implicitly as

$$\frac{d^i S}{dt} = -\int_\Sigma \mathbf{J_s} \cdot \mathbf{n}\, d\Sigma \tag{1.5}$$

$$\frac{d^e S}{dt} = \int_V \sigma_s\, dV. \tag{1.6}$$

Equation 1.6 provides us an interpretation of entropy flux as the amount of entropy flowing through the surface of the body per unit area and unit time, and by 1.5 entropy production can be interpreted as an amount of entropy produced in unit volume per unit time. Further, we have the relation between entropy density from 1.1 and entropy S

$$S = \int_V \rho s\, dV. \tag{1.7}$$

After substituting 1.7, 1.5 and 1.6 into 1.4 we get

$$\frac{d}{dt}\int_V \rho s\, dV = \int_V \sigma_s\, dV - \int_\Sigma \mathbf{J_s} \cdot \mathbf{n}\, d\Sigma, \tag{1.8}$$

[1] Lagrangian time derivative describes how a quantity of some continuum element changes with taking into account also that the motion of the element can change the quantity. It is defined as $d/dt = \partial/\partial t + v \cdot \nabla$.

which can be reformulated using the Gauss theorem, and the fact that Lagrange time derivative of matter density ρ is zero as

$$\int_V \rho \frac{ds}{dt}\, dV = \int_V \sigma_s\, dV - \int_V \nabla \cdot \mathbf{J_s}\, dV. \tag{1.9}$$

As this has to be satisfied for arbitrarily chosen volume V, as integrands are continuous functions, the equation 1.9 must also be satisfied pointwise, therefore it holds

$$\rho \frac{ds}{dt} = \sigma_s - \nabla \cdot \mathbf{J_s}. \tag{1.10}$$

Equation 1.10 tells us that the change of entropy is pointwise given as production of entropy in the respective point and a change of entropy flux in the point. A similar equation can be derived analogically for arbitrary extensive state variable. The equation 1.10 and its analogies also play a fundamental role in deriving the equations for systems, which can be described by CIT. The following section will show how to derive such equations in general.

1.1.3 General structure

Our goal in this section is to determine evolution equations for all the variables describing the system. For an arbitrary system, which can be well described by CIT, we can find a system of equations by following the steps below.

1. **Find a state variables** Write down the list of the parameters of the system that can change. There must always be an even number of parameters (one intensive variable for every extensive variable and vice versa).

2. **Evolution equations** For each extensive state variable A, we can write down analogical derivation as we did in the previous section for entropy S and get the evolution equation for its density a. As a result, the equation will take the form

   $$\rho \frac{da}{dt} = \sigma_a - \nabla \cdot \mathbf{J_a}, \tag{1.11}$$

   where σ_a and $\mathbf{J_a}$ are the production of quantity A (source term) and flux of quantity A, respectively.

3. **Identification of entropy production and entropy flux** In this step, we take evolution equations 1.11 and use them to express the time derivatives in the equation for the lagrangian time derivative of entropy 1.3. After that, we compare the result with 1.10 and identify the entropy flux and entropy production. The entropy production is found in a way that it can be written as

   $$\sigma_s = \sum_{i=1}^{N} J_i X_i, \tag{1.12}$$

   where J_i are thermodynamic fluxes of a_i and X_i are thermodynamic forces, typically associated with the gradient of some functions of intensive variables. Forces and fluxes can generally be scalar, vector, or tensor quantities. As the entropy production is always scalar quantity, $J_i X_i$ stands for product, scalar product or double scalar product between two tensors (for tensors $\mathbf{T}$ and $\mathbf{S}$ defined as $\mathbf{T} : \mathbf{S} = \sum_{a,b} \mathbf{T_{ab}} \mathbf{S_{ab}}$).

4. **Force-flux relations** Empirically, we know that thermodynamical forces and fluxes are dependent on each other. In fact, they are moreover linearly dependent on each other if we are *close enough to the equilibrium*. Moreover, taking fluxes as linear functions of thermodynamical forces

$$J_i = \sum_{j=1}^{N} L_{ij} X_j \tag{1.13}$$

will ensure that the entropy production will be positive (provided that the matrix $\mathbf{L}$ will be positively definite).

5. **Restrictions on $\mathbf{L_{ij}}$** Coefficients L_{ij} can not be arbitrary, but subject to certain restrictions, which are discussed in detail in [10]. The first is that material symmetry reduces the number of coefficients (Curie's law). Second is a restriction on the sign of coefficients, given by the positivity of entropy production, which imply that matrix $\mathbf{L}$ is positive definite. The restriction is caused by time-reversal symmetry and is called Onsager-Casimir's relations. O-C relations state that

$$L_{ij} = L_{ji} \tag{1.14}$$

which means, that $\mathbf{L}$ has to be symmetric matrix.

1.1.4 Simple example: Fourier heat conduction

In this section, we will demonstrate the approach from the previous section on a simple example of deriving equations for heat conduction in a rigid body. We will follow the steps above.

1. **Find a state variables** As the studied object is rigid, V is not a state variable, so the only state variable is U (we will use its density u) and its conjugate T.

2. **Evolution equations** As we have only one extensive variable, we get just one evolution equation for u in shape

$$\rho \frac{du}{dt} = \sigma_u - \nabla \cdot \mathbf{J_u}. \tag{1.15}$$

due to the energy conservation law, no energy can be produced inside the body. Therefore, $\sigma_u = 0$, then as the only way of the internal energy transport is heat conduction, the flux of energy is just heat flux $\mathbf{q}$ moreover, as there is no mass transport inside the body, the lagrangian time derivative simplifies to partial time derivative, which results to

$$\rho \frac{\partial u}{\partial t} = -\nabla \cdot \mathbf{q}. \tag{1.16}$$

3. **Identification of entropy production and entropy flux** We take the evolution equation 1.16 and express the time derivative of u

$$\frac{\partial u}{\partial t} = -\frac{1}{\rho} \nabla \cdot \mathbf{q}. \tag{1.17}$$

Then we take Gibbs equation, which has a shape

$$\frac{\partial s}{\partial t} = \frac{1}{T}\frac{\partial u}{\partial t}, \tag{1.18}$$

where lagrangian derivatives d/dt were replaced with partial derivatives $\partial/\partial t$, for the same reason as in step 2. By plugging 1.17 into 1.18 we get

$$\frac{\partial s}{\partial t} = -\frac{1}{T\rho}\nabla \cdot \mathbf{q}. \tag{1.19}$$

Now we compare time derivative of entropy from 1.10 with 1.19

$$\sigma_s - \nabla \cdot \mathbf{J_s} = -\frac{1}{T}\nabla \cdot \mathbf{q}. \tag{1.20}$$

if we want to identify entropy flux and entropy production (left-hand side), it is hard, as the right-hand side has just one term. Therefore, we try to reformulate the right-hand side using

$$\nabla \cdot \left(\frac{\mathbf{q}}{T}\right) = \frac{1}{T}\nabla \cdot \mathbf{q} + q \cdot \nabla\left(\frac{1}{T}\right) \tag{1.21}$$

we get

$$\sigma_s - \nabla \cdot \mathbf{J_s} = q \cdot \nabla\left(\frac{1}{T}\right) - \nabla \cdot \left(\frac{\mathbf{q}}{T}\right) \tag{1.22}$$

now we see that the first term on the right-hand side corresponds to flux – $\mathbf{q}$ times some gradient of intensive quantity – T, which can be interpreted as a thermodynamic force. That is why we can say that

$$\sigma_s = q \cdot \nabla\left(\frac{1}{T}\right) \tag{1.23}$$

and terms which remained give us

$$\mathbf{J_s} = \frac{\mathbf{q}}{T} \tag{1.24}$$

4. **Force-flux relations** Now we prescribe linear relationship between flux of energy (heat flux) and the respective thermodynamical force.

$$\mathbf{q} = L_{qq}\nabla\left(\frac{1}{T}\right) = -L_{qq}\frac{1}{T^2}\nabla T \tag{1.25}$$

where L_{qq} can be without loss of generality function of T. Defining heat conductivity $\lambda(T) = L_{qq}/T^2$ we can write

$$\mathbf{q} = -\lambda\nabla T, \tag{1.26}$$

which is well-known formulation of Fourier's law. By plugging 1.26 into 1.16 we get

$$\rho\frac{\partial u}{\partial t} = \nabla \cdot (\lambda\nabla T)\,. \tag{1.27}$$

which, using chain rule and definition of heat capacity for constant volume, results in

$$\frac{\partial u}{\partial t} = \frac{\partial u}{\partial T}\frac{\partial T}{\partial t} = c_V \frac{\partial T}{\partial t} \tag{1.28}$$

and assuming constant heat conductivity (which is good approximation of experimental results for not extreme conditions), it can be rewritten as

$$\frac{\partial T}{\partial t} = \kappa \Delta T, \tag{1.29}$$

where we defined heat diffusivity $\kappa = \lambda / \rho c_V$.

5. **Restrictions on $\mathbf{L_{ij}}$** As entropy production given in 1.23 needs to be non-negative, substituting 1.25 for $\mathbf{q}$ in 1.23 we get

$$\sigma_s = L_{qq} \frac{1}{T^4} \left(\nabla T\right)^2 . \tag{1.30}$$

From which, we see that L_{qq} has to be positive. This implies that heat conductivity $\lambda(T) = L_{qq}/T^2$ is also positive. Positive heat conductivity means that due to 1.26 the heat flux has the opposite direction than the temperature gradient, which results in heat flowing from places with higher temperature to places with lower temperature.

In this section, we have shown the derivation of the heat equation from non-equilibrium thermodynamics. We also derived that heat conductivity has to be positive as a consequence of the positivity of entropy production, which is just a generalization of the 2^{nd} law of thermodynamics.

1.2 Transport through the membrane

This section aims to derive water and proton transport equations in a one-dimensional Proton Exchange Membrane (PEM) inside an external electric field. To do so, we will use the theory introduced in the previous section. We will follow the same steps while deriving the heat equation from the principles of CIT.

At first, we must identify the state variables. As the system is isothermal and isobaric, our state variables are Internal energy density u, concentrations of water and protons c_w and c_p and potential energy density u_pot, which is non zero due to applied external electric potential and is given by

$$u_{pot} = \rho_c \varphi_e \tag{1.31}$$

where ρ_c is charge density caused by protons inside the membrane and φ_e is the electric potential of the external electric field. If we now denote $\tilde{u} = u + u_{pot}$ to be the total energy density, we can write down the differential of total energy density

$$d\tilde{u} = Tds + \mu_w dc_w + \mu_p dc_p + \rho_c d\varphi_e + \varphi_e d\rho_c. \tag{1.32}$$

This is just specific form of 1.2, so after taking the time derivative it will be it shape 1.3 which reads

$$\frac{d\tilde{u}}{dt} = T\frac{ds}{dt} + \mu_w \frac{dc_w}{dt} + \mu_p \frac{dc_p}{dt} + \rho_c \frac{d\varphi_e}{dt} + \varphi_e \frac{d\rho_c}{dt}. \tag{1.33}$$

As we want to describe a stationary state with electric potential, which does not change in time, the term with the time derivative of electric potential will be zero. After additional rearrangement 1.33 will have a form

$$\frac{ds}{dt} = \frac{1}{T}\frac{d\tilde{u}}{dt} - \frac{\mu_w}{T}\frac{dc_w}{dt} - \frac{\mu_p}{T}\frac{dc_p}{dt} - \frac{\varphi_e}{T}\frac{d\rho_c}{dt}. \tag{1.34}$$

The second step is to formulate evolution equations for densities of extensive variables $\tilde{u}$, c_w, c_p and ρ_c. As there is no production of protons, water, energy, or charge inside the membrane, equations read

$$\rho\frac{d\tilde{u}}{dt} = -\nabla\cdot\mathbf{J}_{\tilde{\mathbf{u}}} \tag{1.35}$$

$$\rho\frac{dc_w}{dt} = -\nabla\cdot\mathbf{J}_{\mathbf{w}} \tag{1.36}$$

$$\rho\frac{dc_p}{dt} = -\nabla\cdot\mathbf{J}_{\mathbf{p}} \tag{1.37}$$

$$\rho\frac{d\rho_c}{dt} = -\nabla\cdot\mathbf{j}, \tag{1.38}$$

where $\mathbf{J}_{\tilde{\mathbf{u}}}$, $\mathbf{J}_{\mathbf{w}}$ and $\mathbf{J}_{\mathbf{p}}$ are fluxes of total energy, water and protons respectively and $\mathbf{j}$ is current density. As electric current inside the membrane is caused only by the motion of protons, we can write a relationship between $\mathbf{J}_{\mathbf{p}}$ and $\mathbf{j}$

$$\mathbf{J}_{\mathbf{p}} = \frac{\mathbf{j}}{F}, \tag{1.39}$$

where F is Faraday constant.

The third step is to find entropy production and entropy flux. To do this, we have to substitute time derivatives from equations 1.35 – 1.38 in to 1.34 where we get

$$\frac{ds}{dt} = -\frac{1}{T\rho}\left(\nabla\cdot\mathbf{J}_{\tilde{\mathbf{u}}} + \mu_w\nabla\cdot\mathbf{J}_{\mathbf{w}} + \mu_p\nabla\cdot\mathbf{J}_{\mathbf{p}} + \varphi_e F\,\nabla\cdot\mathbf{J}_{\mathbf{P}}\right). \tag{1.40}$$

You may notice that in the last term, we used 1.39 to get rid of the current density to reduce the number of unknown variables. We also want to get rid of the time derivative of entropy density, which we can do by substituting the time derivative from 1.10 instead of the left-hand side. That results in

$$\sigma_s - \nabla\cdot\mathbf{J}_{\mathbf{s}} = -\frac{1}{T}\left(\nabla\cdot\mathbf{J}_{\tilde{\mathbf{u}}} + \mu_w\nabla\cdot\mathbf{J}_{\mathbf{w}} + \mu_p\nabla\cdot\mathbf{J}_{\mathbf{p}} + \varphi_e F\,\nabla\cdot\mathbf{J}_{\mathbf{P}}\right). \tag{1.41}$$

Now we will use the same trick as while deriving the heat equation in the previous chapter. To be more precise, if we have two space-dependent variables A and $\mathbf{B}$ where first is scalar and second is a vector, we can write

$$A\,\nabla\cdot\mathbf{B} = \nabla\cdot(A\mathbf{B}) - \nabla A\cdot\mathbf{B} \tag{1.42}$$

as the left-hand side has the same shape as all terms with a divergence of flux in 1.41, we can use it to express all divergence terms in the same way as in 1.42. That leads to the equation

$$\begin{aligned}\sigma_s - \nabla\cdot\mathbf{J}_{\mathbf{s}} = {}& \nabla\cdot\left(-\frac{\mathbf{J}_{\tilde{\mathbf{u}}}}{T} + \frac{\mathbf{J}_{\mathbf{w}}\mu_w}{T} + \frac{\mathbf{J}_{\mathbf{p}}\mu_p}{T} + \frac{\mathbf{J}_{\mathbf{p}}\varphi_e F}{T}\right)\\ & + \mathbf{J}_{\tilde{\mathbf{u}}}\cdot\nabla\left(\frac{1}{T}\right) - \mathbf{J}_{\mathbf{w}}\cdot\nabla\left(\frac{\mu_w}{T}\right) - \mathbf{J}_{\mathbf{p}}\cdot\nabla\left(\frac{\mu_p}{T}\right) - \mathbf{J}_{\mathbf{p}}\cdot\nabla\left(\frac{\varphi_e F}{T}\right).\end{aligned} \tag{1.43}$$

In 1.43 we can easily identify entropy production as

$$\sigma_s = \mathbf{J_{\tilde{u}}} \cdot \nabla \left(\frac{1}{T}\right) - \mathbf{J_w} \cdot \nabla \left(\frac{\mu_w}{T}\right) - \mathbf{J_p} \cdot \nabla \left(\frac{\mu_p}{T}\right) - \mathbf{J_p} \cdot \nabla \left(\frac{\varphi_e F}{T}\right). \tag{1.44}$$

A whole system is isothermal, the first term on the right-hand side vanishes, and after some rearrangement, we get

$$\sigma_s = -\frac{1}{T}\left(\mathbf{J_w} \cdot \nabla \mu_w + \mathbf{J_p} \cdot \nabla \tilde{\mu}_p\right), \tag{1.45}$$

where we introduced $\tilde{\mu}_p$ to be the electrochemical potential generally defined as

$$\tilde{\mu}_p = \mu_p + z\varphi_e F \tag{1.46}$$

where z is a charge of the described particle in units of the elementary charge. As we are talking about the electrochemical potential of protons, we have $z = 1$.

The fourth step is to write down the force-flux relations, which are the equations we want to solve in this work. Using the assumption that the fluxes are linear functions of forces, we can write down the following equations

$$\mathbf{J_p} = -\frac{L_{pp}}{T}\nabla\tilde{\mu}_p - \frac{L_{pw}}{T}\nabla\mu_w \tag{1.47}$$

$$\mathbf{J_w} = -\frac{L_{wp}}{T}\nabla\tilde{\mu}_p - \frac{L_{ww}}{T}\nabla\mu_w, \tag{1.48}$$

where minuses have to be added to make the entropy production positive.

As in this masters thesis, we are solving only one dimensional model of PEM fuel cell, [2] we will change the notation for simplicity. The one-dimensional fluxes $\mathbf{J_w}$ and $\mathbf{J_p}$ can be replaced with scalars j_w and j_p respectively. Also, the vector operator ∇ can be replaced with one-dimensional form $\partial/\partial x$. However, we will keep it in its current form for simplicity of notation.

Now we will take a look at the electrochemical potential $\tilde{\mu}_p$ for a while. The usual way we can measure the electrochemical potential of protons is using a voltmeter [11]. That leads to the more natural choice of units for the electrochemical potential of protons, which are Volts. Also, we will introduce a new notation for the electrochemical potential of protons $\tilde{\mu}_p := \phi$ as it has the same units and is measured in the same way as the electrostatic potential. These two changes together will change the equations to the form

$$j_p = -\frac{L_{pp}F}{T}\nabla\phi - \frac{L_{pw}}{T}\nabla\mu_w \tag{1.49}$$

$$j_w = -\frac{L_{wp}F}{T}\nabla\phi - \frac{L_{ww}}{T}\nabla\mu_w, \tag{1.50}$$

where Faraday constant F has to be added to compensate for the change of units, in the same way as in 1.46.

Our goal is to formulate the equations in a form that uses the most natural variables. The chemical potential of water can not be measured directly, but

[2] Which is sufficient to describe the experiment, which was on purpose constructed in a way that its description should be fully covered by one-dimensional theory – will be discussed more in-depth in the later chapter.

on the other hand, we can associate the chemical potential of water with water activity a_w by using ([12])

$$\mu_w = \mu_w^0 + RT\log(a_w). \tag{1.51}$$

Water activity is a quantity equivalent to relative humidity for various materials. It is defined as the ratio of water vapor pressure and saturated vapor pressure at the same temperature. If the material is some gas, water activity and relative humidity are the same. Using the definition for 1.51 we can rewrite the force X_w as

$$X_w = -\frac{1}{T}\nabla\mu_w = -R\nabla\left(\log(a_w)\right) = -R\frac{\nabla a_w}{a_w}. \tag{1.52}$$

By using this new formulation for X_w after plugging it into 1.49 and 1.50 we get

$$j_p = -\frac{L_{pp}F}{T}\nabla\phi - RL_{pw}\frac{\nabla a_w}{a_w} \tag{1.53}$$

$$j_w = -\frac{L_{wp}F}{T}\nabla\phi - RL_{ww}\frac{\nabla a_w}{a_w}, \tag{1.54}$$

which is the system of equations for transport inside the PEM membrane in its most natural variables. However, the real difficulty lies in determining the coefficients L_{ij}. The following section will focus on determining the coefficients from experimentally measurable quantities.

1.3 Coefficients L_{ij}

1.3.1 Determining the coefficients

Phenomenological coefficients are determined from indirect measurements experimentally. In this case, they can be determined from measurements *proton conductivity, water diffusivity water concentration* and *drag coefficient*. In this section, we will derive how coefficients can be connected with mentioned measurable quantities.

Before we will do this, we will rewrite the force-flux relations 1.49 1.50 in a different shape. Denoting thermodynamical forces $X_p = \frac{F}{T}\nabla\phi$ and $X_w = \frac{1}{T}\nabla\mu_w$, the equations will take the form

$$j_p = L_{pp}X_p + L_{pw}X_w \tag{1.55}$$

$$j_w = L_{wp}X_p + L_{ww}X_w, . \tag{1.56}$$

when we express X_p from 1.55 and substitute it into 1.56 and also X_w from 1.56 and substitute it into 1.55, we get

$$j_p = \frac{L_{ww}L_{pp} - L_{wp}L_{pw}}{L_{ww}}X_p + \frac{L_{wp}}{L_{ww}}j_w \tag{1.57}$$

$$j_w = \frac{L_{ww}L_{pp} - L_{wp}L_{pw}}{L_{pp}}X_w + \frac{L_{wp}}{L_{pp}}j_p. \tag{1.58}$$

Proton conductivity σ_p is defined as

$$\sigma_p = \frac{F^2}{T}\left(\frac{j_p}{X_p}\right)_{X_w=0}, \tag{1.59}$$

where the flux j_p is expressed in $mol \cdot s^{-1} \cdot m^{-2}$, X_p is expressed in $V \cdot m^{-1} \cdot s \cdot A \cdot mol^{-1} \cdot K^{-1}$ and σ_p in Sm^{-1}. Using the equation 1.55 for j_p, after setting the $X_w = 0$ it gives us

$$\sigma_p = \frac{F^2}{T} L_{pp}. \tag{1.60}$$

Which is direct relationship between L_{pp} and experimentally measurable proton conductivity.

Water Diffusivity D_w and *water concentration* c_w are defined as

$$\frac{D_w c_w}{R} = \left(\frac{j_w}{X_w}\right)_{j_p=0} \tag{1.61}$$

where the water flux j_w is expressed in $mol \cdot s^{-1} \cdot m^{-2}$, X_w is expressed in $J \cdot mol^{-1} \cdot m^{-1} \cdot K^{-1}$ and D_w, c_w in $m^2 \cdot s^{-1}$ and $mol \cdot m^3$ respectively. When we use the expression of j_w from 1.58 and substitute it into 1.61 we get

$$\frac{D_w c_w}{R} = \frac{L_{ww} L_{pp} - L_{wp} L_{pw}}{L_{pp}} = L_{ww} - \frac{L_{wp} L_{pw}}{L_{pp}}. \tag{1.62}$$

Drag coefficient is a quantity that expresses how the proton flux affects the water flux. This coefficient is defined as a ratio of the fluxes under the condition of zero thermodynamical force acting on the water X_w. It reads

$$\xi = \left(\frac{j_w}{j_p}\right)_{X_w=0}, \tag{1.63}$$

which can be using the equation 1.58 for j_w rewritten as

$$\xi = \frac{L_{wp}}{L_{pp}} \tag{1.64}$$

as the first term in 1.58 vanishes due to $X_w = 0$.

After we obtain experimentally measured values of σ_p, D_w, c_w and ξ we still have just three equations (1.64, 1.62, 1.60) to express four coefficients L_{ij}. However, no other measurements are needed, as we can make use of Onsager-Casimir reciprocal relations (OCRR) mentioned in 1.14. Thanks to that, we have another equation $L_{pw} = L_{wp}$ and therefore, we can use just one cross coefficient L_{cross} instead of them. Using this new notation, we can express L_{pp}, L_{ww} and L_{cross} in terms of measurable quantities as

$$L_{pp} = \frac{T}{F^2} \sigma_p \tag{1.65}$$

$$L_{cross} = \frac{T\xi}{F^2} \sigma_p \tag{1.66}$$

$$L_{ww} = \frac{D_w c_w}{R} + \frac{T\xi^2}{F^2} \sigma_p. \tag{1.67}$$

In general, all measurable quantities σ_p, D_w, c_w, and ξ can be a function of pressure, temperature, and water activity in the membrane. During the experiments, pressure and temperature were kept constant. In our model, we can assume that they are just functions of water activity. It is, however, possible to derive one another restriction on the shape of the L_{ij} coefficients. This will be shown in the next section.

1.3.2 Functional Constraints

In this section, we will reproduce the derivation of functional constraints on phenomenological coefficients from the article [13]. Consider a system described by the one-dimensional CIT theory. Consider additionally that the system is relaxed to the stationary state, where all the fluxes are spatially constant. Additionally, we will assume a system with two state variables x_1 and x_2, two respective fluxes j_1, j_2 and two respective thermodynamical forces X_1, X_2. The flux-force relations will have the same shape as 1.55 and 1.56, which reads

$$j_1 = L_{11}X_1 + L_{12}X_2 \tag{1.68}$$
$$j_2 = L_{21}X_1 + L_{22}X_2, . \tag{1.69}$$

Another assumption we need is that when one thermodynamical force, (without loss of generality let it be X_2) vanishes everywhere due to setting appropriate boundary conditions for x_2, the other will not vanish. Last assumption needed is that the coefficients are not functions of x_2. [3]

Under this circumstances, let us assume we can set boundary conditions for x_2 as $x_2|_{x=0} = x_2|x = L = c_1$, such that $X_2 = 0$. As X_2 is proportional to the gradient of x_2, x_2 must be constant for all x. Now we express the ratio of j_1 and j_2

$$\frac{j_1}{j_2} = \frac{L_{11}}{L_{21}}. \tag{1.70}$$

Due to j_1 and j_2 are both constant, the ratio of L_{11} and L_{21} is constant. This means, that both L_{11} and L_{21} must have the same functional dependence on the state variable x_1. By OCRR 1.14 we see that also L_{12} has the same functional dependence on x_1.

Next, we want to show that also L_{22} has the same functional dependence as the other coefficients, and we can write the equations 1.68 and 1.69 as

$$\begin{pmatrix} j_1 \\ j_2 \end{pmatrix} = f(x_1) \begin{pmatrix} \tilde{L}_{11} & \tilde{L}_{12} \\ \tilde{L}_{21} & \tilde{L}_{22} \end{pmatrix} \begin{pmatrix} X_1 \\ X_2 \end{pmatrix}, \tag{1.71}$$

where $\tilde{L}_{11}$, $\tilde{L}_{12}$, $\tilde{L}_{21}$ and $\tilde{L}_{22}$ can be only functions of x_2 and $f(x_1)$ denotes the functional dependence of coefficients on x_1.

Let us denote f_1 the functional dependence of L_{22} on x_1. Assuming that the f_1 is monotonous function, we can write $x_1 = f_1^{-1}(L_{22})$. Further, we introduce the notation

$$f(x_1) = f(f_1^{-1}(L_{22})) = f_2(L_{22}) \tag{1.72}$$

and all the coefficients can be written as a function of L_{22}. Due to the second law of thermodynamics, we have that the matrix L_{ij} must be positive definite. This is satisfied for $L_{11} > 0$ $L_{22} > 0$ and $L_{11}L_{22} - L_{12}L_{21} > 0$. The latter equation can be rewritten in terms of 1.72 as

$$f_2(L_{22}) \left(\tilde{L}_{11}L_{22} - \tilde{L}_{12}^2 f_2(L_{22}) \right) > 0. \tag{1.73}$$

[3] This assumption may be unnecessary, as It is possible, that it follows from the previous one. However, if there is an implication between the penultimate assumption and last assumption, it is not straightforward. Therefore, we said it as a separate assumption.

$\tilde{L}_{11}$ and $\tilde{L}_{12}$ can have for different thermodynamic systems different values, which does not depend on L_{22}. Without loss of generality, we can further choose $f_2(L_{22})$ to be positive for all $L_{22} > 0$. This will uniquely determine the signs of $\tilde{L}_{11}$ and $\tilde{L}_{12}$. If we assume f_2 is an analytic function and can be written as

$$f_2(L_{22}) = \sum_{n=0}^{\infty} a_n L_{22}^n. \tag{1.74}$$

For sufficiently small values of L_{22} the 1.73 reads

$$f_2(L_{22}) \left(\tilde{L}_{11} L_{22} - \tilde{L}_{12}^2 f_2(L_{22})\right) \approx -\tilde{L}_{12}^2 a_0^2 > 0, \tag{1.75}$$

which holds just for $a_0 = 0$. Using the fact that $f_2(L_{22}) > 0$ we can rewrite 1.73 as

$$\left(\tilde{L}_{11} L_{22} - \tilde{L}_{12}^2 f_2(L_{22})\right) > 0. \tag{1.76}$$

$$\tilde{L}_{11} L_{22} > \tilde{L}_{12}^2 f_2(L_{22}). \tag{1.77}$$

This can be true for all L_{22} just if $a_n = 0$ for all $n > 1$. Therefore, we have $f_2(L_{22}) = a_1 L_{22}$. Using 1.72 we get

$$f(x_1) = f_2(L_{22}) = a_1 L_{22} \tag{1.78}$$

which means, that L_{22} has same functional dependence on x_1 as the other coefficients.

We will use the functional constraints for the system of equations describing proton and water flux inside the PEM membrane. Let a_w and ϕ be the x_1 and x_2 respectively. As the electric potential is given uniquely up to a constant, the coefficients can not depend on its value (satisfying the last assumption). Therefore, all the coefficients will be the same function of a_w and measured quantities D_w, c_w and σ_p will be just functions of water activity a_w. Moreover, functional constraints tell us that the drag coefficient ξ, which is defined as a ratio of L_{cross} and L_{pp} must be constant for all water activities. Above mentioned allows us then to write flux-force relations 1.49 and 1.50 in a form

$$\begin{pmatrix} j_p \\ j_w \end{pmatrix} = \frac{f(a_w)}{T} \begin{pmatrix} \tilde{L}_{pp} & \tilde{L}_{cross} \\ \tilde{L}_{cross} & \tilde{L}_{ww} \end{pmatrix} \begin{pmatrix} -F\nabla\phi \\ -RT\frac{\nabla a_w}{a_w}, \end{pmatrix} \tag{1.79}$$

which will after plugging in the 1.65, 1.66 and 1.67 gives us

$$\begin{pmatrix} j_p \\ j_w \end{pmatrix} = \frac{f(a_w)}{F^2} \begin{pmatrix} \sigma_p^0 & \sigma_p^0 \xi \\ \sigma_p^0 \xi & \frac{L_{dif} F^2}{RT} + \sigma_p^0 \xi^2 \end{pmatrix} \begin{pmatrix} -F\nabla\phi \\ -RT\frac{\nabla a_w}{a_w}, \end{pmatrix} \tag{1.80}$$

where L_{dif} and σ_p^0 are constants such that

$$\sigma_p = \sigma_p^0 f(a_w) \tag{1.81}$$

$$D_w c_w = L_{dif} f(a_w). \tag{1.82}$$

1.3.3 Stationary states

In this thesis, we will describe the membrane in the stationary state. We call some state of the system to be stationary if all the state variables, velocities, and fluxes do not change in the course time. A good example can be an electric heater, to which a constant electrical power is supplied, and its temperature remains unchanged. (The temperature does not change due to heat losses by radiation and heat conduction. The losses are the same as the gain from its heating.) The stationary state differs from the equilibrium state (which can be the same heater, but after the electricity supply is turned off and the heater equilibrates with the surroundings). Although in both cases, the state variables (in this case, the temperature is the only state variable) are constant, in the first case, there are non-zero heat fluxes and heat productions (which are both constant in time).

It can be shown (precise derivation can be found in [10]) that entropy production decreases over time and that it reaches its minimum in a state which has to be stationary. In the case of water and proton transport through the membrane, after changing the boundary conditions, the system always relaxes to some stationary state, where state variables (water activity and electrochemical potential of protons) will be time-independent functions, and the fluxes will be constant. Constant fluxes can also be viewed as s consequence of balance equations 1.36 and 1.37 where when the concentration of species in the membrane does not evolve in time, then the left-hand side is zero, which implies that fluxes have to be constant. Therefore, we will be solving the equations inside the membrane

$$\nabla j_p = 0 \tag{1.83}$$

$$\nabla j_w = 0, \tag{1.84}$$

for j_p and j_w defined by 1.80

1.4 Equations on the electrodes

In this section we are going to derive expressions for the fluxes through the boundary. To derive the expression for proton flux, we need to introduce the basics of the theory of the electrochemical reactions first. In this section, we will derive expressions for the fluxes through the boundary. To derive the expression for proton flux, we need to introduce the basics of the theory of the electrochemical reactions first.

1.4.1 Electrochemical reactions

In contrast to chemical reactions, electrochemical reactions involve the transport of the ions subjected to the electric field. Let us assume a typical electrochemical reaction where species A_2B_2 are reduced to two charged species A^+ and two charged species B^- and vice versa

$$\mathrm{A_2B_2} \longleftrightarrow 2\,\mathrm{A^+} + 2\,\mathrm{B^-} \tag{1.85}$$

The number standing before some reactant or product is called a stoichiometric coefficient. In this case, stoichiometric coefficients of $\mathrm{A^+}$ and $\mathrm{B^+}$ are 2 and stoichiometric coefficient of $\mathrm{A_2B_2}$ is 1.

So far, we know that the flux of species (we derived it for protons and water) is proportional to the gradient of its electrochemical potential (which reduces to the chemical potential for species without electric charge). Analogically, the difference in electrochemical potential between reactants and products is the quantity that determines the speed and direction of electrochemical reaction [12]. To be more precise, we introduce a new quantity, called overpotential η, defined as

$$\eta = \frac{\tilde{\mu}_{prod} - \tilde{\mu}_{react}}{FN_q} = \frac{\Delta\tilde{\mu}}{FN_q} \tag{1.86}$$

where $\tilde{\mu}_{prod}$ and $\tilde{\mu}_{react}$ are the electrochemical potential of all products and electrochemical potential of all reactants, respectively, and N_q is the number of negative or positive elementary charges (the number must be the same) involved in the reaction. As can be seen from 1.86 overpotential is the amount of Gibbs energy of reaction normalized to the transition of one ion with elementary charge.

If the overpotential is positive the reaction proceeds forward $\mathrm{A_2B_2} \longrightarrow 2\,\mathrm{A^+} + 2\,\mathrm{B^-}$ and if it is negative, it proceeds backwards $\mathrm{A_2B_2} \longleftarrow 2\,\mathrm{A^+} + 2\,\mathrm{B^-}$. Note that this notation is invariant with respect to the initial choice of reactants and products. After switching reactants with products, the sign of overpotential will change, and the reaction will proceed in the direction as before.

Now we know what drives the reaction to one side or another, but we do not understand how exactly overpotential affects the reaction speed. That is very hard to derive rigorously. However, for this purpose, the Buttler-Volmer equation is used [11] as it is in good agreement with experimental data. The Buttler-Volmer equation for the production rate of species A reads

$$j_A = j_0 \left(e^{(1-\alpha)N_A\eta F/RT} - e^{-\alpha N_A \eta F/RT} \right) \tag{1.87}$$

where j_0 is a constant called exchange current specific for every reaction and depends on given conditions (temperature and pressure), N_A is a stoichiometric coefficient of A and α is the transfer coefficient, which lies in the interval $(0, 1)$ and is typically a fitted parameter of the described system.

1.4.2 HOR and HRR reactions

In our experiment, the hydrogen oxidation reaction HOR proceeds on one side of the membrane, and on the other, the hydrogen reduction reaction HRR takes place. They are the same reactions in which gaseous hydrogen on the electrode (placed on the surface of the membrane) dissociates to protons and electrons on one side, and electrons and protons reduce to gaseous hydrogen on the other.

$$\mathrm{H_2} \longleftrightarrow 2\,\mathrm{H^+} + 2\,\mathrm{e^-} \tag{1.88}$$

Using the equation 1.86 we can write down the overpotential for HOR reaction

$$\eta_{HOR} = \frac{1}{2F}\left(\tilde{\mu}_{H_2} - 2\tilde{\mu}_{H^+} - 2\tilde{\mu}_{e^-}\right) \tag{1.89}$$

$$= \frac{1}{2F}\left(\tilde{\mu}^o_{H_2} + RT\log\left(\frac{p_{H_2}}{p^o}\right) - 2F\phi + 2F\phi_{e^-}\right) \tag{1.90}$$

$$= \frac{RT}{2F}\log\left(\frac{p_{H_2}}{p^o}\right) - \phi + \phi_{e^-}, \tag{1.91}$$

where we again denoted the electrochemical potential of protons as ϕ and for consistency of notation, we also denoted the electrochemical potential of electrons ϕ_{e^-}. As the experimental setup was isobaric at pressure $p = p^o$, we can assume that hydrogen and water are ideal gases and that they are the only compounds of gas in the setup. Therefore, we can write $p^o = p_{H_2} + p_{H_2O}$, which gives us

$$\eta_{HOR} = \frac{RT}{2F} \log\left(\frac{p_{H_2}}{p^o}\right) - \phi + \phi_{e^-} \tag{1.92}$$

$$= \frac{RT}{2F} \log\left(\frac{p^o - p_{H_2O}}{p^o}\right) - \phi + \phi_{e^-} \tag{1.93}$$

$$= \frac{RT}{2F} \log\left(1 - \frac{p_{H_2O}}{p^o}\right) - \phi + \phi_{e^-} \tag{1.94}$$

$$= \frac{RT}{2F} \log\left(1 - \frac{p_{H_2O}}{p^o}\frac{p_{sat}}{p_{sat}}\right) - \phi + \phi_{e^-} \tag{1.95}$$

$$= \frac{RT}{2F} \log\left(1 - RH\frac{p_{sat}}{p^o}\right) - \phi + \phi_{e^-} \tag{1.96}$$

where RH stands for Relative Humidity, which is defined as a ratio of water vapor pressure p_{H_2O} and saturated vapor pressure p_{sat} and is interchangeable with water activity a_w under standard atmospheric pressure ([14]).

The overpotential for HRR reaction has to be the same. The only difference is its sign

$$\eta_{HOR} = -\eta_{HRR} \tag{1.97}$$

In the experiments, we were not deciding which reaction took place on the electrode directly. We could adjust the applied electric potential [4] U. As the electric potential is defined up to a constant, we can, without loss of generality, set it to be 0 on the right electrode and U on the left electrode (U can be positive or negative during the experiments). [5]. In the model, the left electrode lies at the point $x = 0$ and the right electrode at $x = L$. With this notation, we get the final expression for overpotential on both electrodes as

$$\eta|_{x=0} = \frac{RT}{2F} \log\left(1 - RH|_{x=0^-} \cdot p_{sat}\right) - \phi|_{x=0^+} + U \tag{1.98}$$

$$\eta|_{x=L} = \frac{RT}{2F} \log\left(1 - RH|_{x=L^+} \cdot p_{sat}\right) - \phi|_{x=L^-}, \tag{1.99}$$

where p_{sat} is expressed in the units of standard atmospheric pressure p^o and $|_{x=0^-}$ means the value on the left side of the electrode (In case of $x = 0$, it is outside the membrane) and $|_{x=0^+}$ means the value on the right side of the electrode (In case of $x = 0$ it is inside the membrane).

[4] Naturally, the ϕ and ϕ_{e^-} are zero; therefore, the overpotential is very small, as it is only given by different pressures of hydrogen on the opposite sites of the membrane. If we want to study the transport through the membrane under different conditions, we have to moderate the proton flux artificially. That is made by applying some external electric potential to the electrodes. The applied electric potential is then associated with the electrochemical potential of electrons.

[5] The role of the electrodes as the anode and the cathode changes while changing applied potential U. Therefore in this thesis, we use the notation of electrodes as "left" and "right."

As all protons produced on the anode immediately start to move through the boundary, the proton flux prescribed on the boundary is equal to the production rate of the reaction given by the Butler-Volmer equation 1.87. The final expression for proton fluxes on the electrode is then using $\alpha = 1/2$

$$j_{H^+}|_{x=0} = -j_0 \sinh\left(\eta|_{x=0}\frac{F}{RT}\right) \tag{1.100}$$

$$j_{H^+}|_{x=L} = j_0 \sinh\left(\eta|_{x=L}\frac{F}{RT}\right). \tag{1.101}$$

Where minus sign in equation 1.100 is since the normal vector of the boundary for $x = 0$ points to the $-x$ direction. It can be seen that the sign is correct because the flux of protons from on one side must have the same direction as on the other side (as protons are not produced or destroyed inside the membrane). And only additional difference between 1.100 and 1.101 is that the overpotential inside 1.100 has opposite sign as the overpotential in 1.101. This means that, either $\eta|_{x=0}$ is negative and then $j_{H^+}|_{x=0} = j_{H^+}|_{x=L}$ and both are positive, or $\eta|_{x=L}$ is negative and then $j_{H^+}|_{x=0} = j_{H^+}|_{x=L}$ and both are negative.

1.4.3 Equations for water flux through the boundary

For water flux, the boundary conditions are prescribed as ([15])

$$j_w|_{x=0} = k_w(a_w|_{mem.} - a_w|_{out.}) \tag{1.102}$$

$$j_w|_{x=L} = k_w(a_w|_{out.} - a_w|_{mem.}), \tag{1.103}$$

where k_w is a phenomenological constant, which is determined experimentally and differs for different experimental setups, and $a_w|_{mem.}$ and $a_w|_{out.}$ are water activities on the electrode inside the membrane and outside the membrane, respectively. The equations 1.102 and 1.103 are given empirically, as water flux is a linear function of the water activity drop over the interface. The water activity $a_w|_{out.}$ is equal to the relative humidity RH of the hydrogen on the electrode from the outer side. Therefore, we can rewrite 1.102 and 1.103 as

$$j_w|_{x=0} = k_w(a_w|_{mem.} - RH|_{x=0^-}) \tag{1.104}$$

$$j_w|_{x=L} = k_w(RH|_{x=L^+} - a_w|_{mem.}),. \tag{1.105}$$

1.5 Analytical solution

We found out that if we focus only on the system of equations inside the membrane (not considering any boundary conditions for a while), it can be solved analytically. Although we will be then unable to find the right integration constants due to no boundary equations, the character of the solution can tell us whether there could be problems with the numerical implementation (for example, if the solution heavily oscillates or if it has singularities, it could be the problem to solve the system numerically). We will take the equations in the form 1.80. As we are looking for the stationary state solution, we want the divergence of both fluxes to be zero, as follows from 1.83 and 1.84. As the problem is one

dimensional, after taking the derivative with respect to x of 1.80 and setting it equal to zero, we get

$$\begin{pmatrix} \sigma_p^0 & \sigma_p^0\xi \\ \sigma_p^0\xi & \frac{L_{dif}F^2}{RT} + \sigma_p^0\xi^2 \end{pmatrix} \left(\frac{f(\mathrm{e}^\nu)}{F^2} \begin{pmatrix} -F\partial_{x^2}\phi \\ -RT\partial_{x^2}\nu \end{pmatrix} + \mathrm{e}^\nu\, \partial_x\nu\, \frac{f^{'}(\mathrm{e}^\nu)}{F^2} \begin{pmatrix} -F\partial_x\phi \\ -RT\partial_x\nu \end{pmatrix} \right) = 0, \tag{1.106}$$

where we instead of the function $a_w(x)$ use the function $\nu(x)$ defined as $a_w = \mathrm{e}^{\nu(x)}$.

Because the matrix in 1.106 is constant, we can multiply the equation by its inverse (inverse matrix must exist as the matrix $\mathbf{L}$ is positively definite) and get

$$\frac{f(\mathrm{e}^\nu)}{F^2} \begin{pmatrix} -F\partial_{x^2}\phi \\ -RT\partial_{x^2}\nu \end{pmatrix} + \mathrm{e}^\nu\, \partial_x\nu\, \frac{f^{'}(\mathrm{e}^\nu)}{F^2} \begin{pmatrix} -F\partial_x\phi \\ -RT\partial_x\nu \end{pmatrix} = 0. \tag{1.107}$$

the second equation in the system 1.107 is ODE with one unknown function, so we can try to solve it. The equation is analytically solvable only for some functions f. However, it can be shown that the measured functions f can be for a chosen interval of a_w approximated with satisfying precision by a $f(a_w) \approx k \cdot a_w^\alpha$, where α and k depends on the chosen interval. In terms of the function $\nu(x)$, we have

$$f(\mathrm{e}^{\nu(x)}) \approx k \cdot \mathrm{e}^{\alpha\nu(x)}. \tag{1.108}$$

After plugging 1.108 into 1.107 and dividing by the constant k we get

$$\frac{\mathrm{e}^{\alpha\nu}}{F^2} \begin{pmatrix} -F\partial_{x^2}\phi \\ -RT\partial_{x^2}\nu \end{pmatrix} + \alpha\mathrm{e}^\nu\, \partial_x\nu\, \frac{\mathrm{e}^{(\alpha-1)\nu)}}{F^2} \begin{pmatrix} -F\partial_x\phi \\ -RT\partial_x\nu \end{pmatrix} = 0. \tag{1.109}$$

Taking the second equation from 1.109 and multiplying by $-F^2/RT\mathrm{e}^{-\alpha\nu}$ we get

$$\partial_{x^2}\nu(x) + \alpha(\partial_x\nu(x))^2 = 0 \tag{1.110}$$

We will now introduce a new function $\mu = (\partial_x\nu$ which leads to

$$\partial_x\mu(x) + \alpha\mu(x)^2 = 0, \tag{1.111}$$

which can be solved by the separation of variables then after integrating $\mu(x)$ we get the result for $\nu(x)$, which reads

$$\mu(x) = \frac{1}{\alpha x + c_1} \tag{1.112}$$

$$\nu(x) = \frac{\log(\alpha x + c_1)}{\alpha} + c_2. \tag{1.113}$$

Now we will solve the first equation. Again we multiply by $-F\mathrm{e}^{-\alpha\nu}$ and get

$$\partial_{x^2}\phi + \alpha\partial_x\nu\partial_x\phi = 0. \tag{1.114}$$

Again we will use the substitution in a form $\partial_x\phi = \varphi$ and plug in the μ for the $\partial_x\nu$

$$\partial_x\varphi + \frac{\alpha}{\alpha x + c_1}\varphi = 0. \tag{1.115}$$

The 1.115 can be again solved by separation of variables which gives us results for φ and by integrating the expression for φ also the expression for ϕ, which reads

$$\varphi(x) = \frac{c_3}{\alpha x + c_1} \tag{1.116}$$

$$\phi(x) = c_3 \frac{\log(\alpha x + c_1)}{\alpha} + c_4. \tag{1.117}$$

.

So the resulting equations for ϕ and a_w (which will be obtained after taking the exponential of 1.113) are

$$a_w(x) = C_2(\alpha x + C_1)^{1/\alpha} \tag{1.118}$$

$$\phi(x) = C_3 \frac{\log(\alpha x + C_1)}{\alpha} + C_4, \tag{1.119}$$

where $C_1 = c_1$, $C_3 = c_3$, $C_4 = c_4$ and $C_2 = \exp(c_2)$. As α is strictly greater than 1 (as can be seen from figure 1.1), the numerical calculations of the water activity profile 1.118 can be problematic as its derivative approaches infinity for $\alpha x \approx -C_1$. For the same value of x, the electrochemical potential of protons will diverge, as can be seen from 1.119. Although we do not know the water activity profile and electrochemical potential profile in the membrane, we know that there possibly can be a problem numerically. We also know that it will be in the same place in the membrane for both functions.

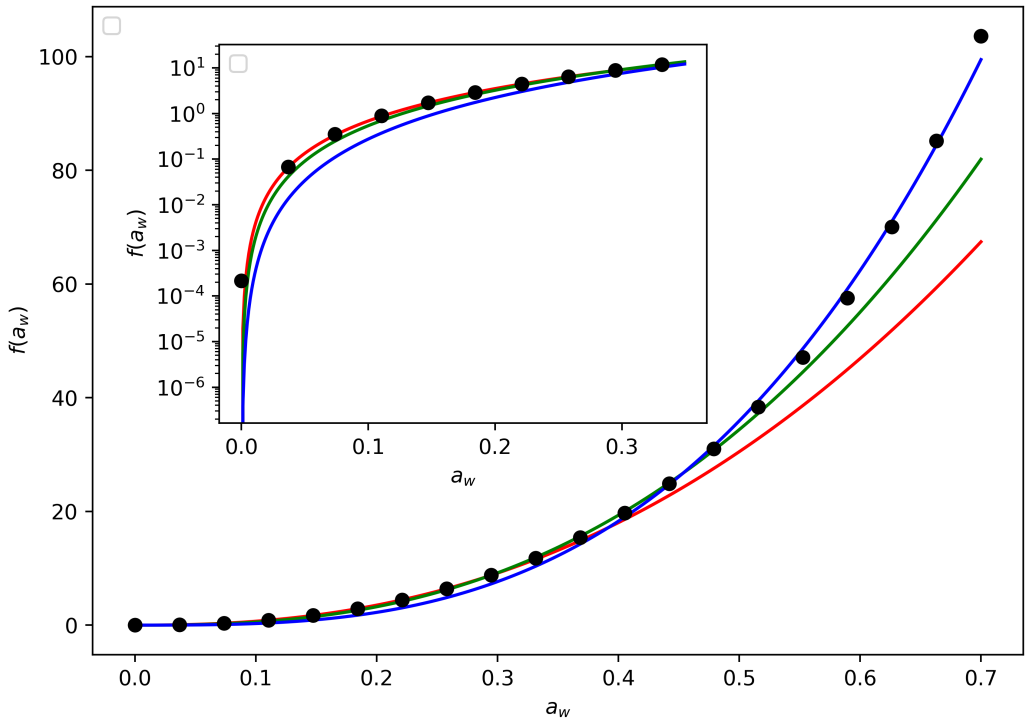

Figure 1.1: The figure shows how the measured dependence of phenomenological coefficients on a_w can be fitted with a function in a shape $k \cdot a_w^{\alpha}$. The red curve shows the best fit for $f(a_w)$ in range 0 – 0.3, the green curve shows the best fit for range 0 – 0.5 and the blue curve shows the best fit for range 0 – 0.7. The fitted values of coefficients are $k = 156.3 \pm 0.1$, $\alpha = 2.357 \pm 2 \cdot 10^{-6}$ for red curve, $k = 205.7 \pm 0.6$, $\alpha = 2.581 \pm 2 \cdot 10^{-5}$ for green curve and $k = 293 \pm 2$, $\alpha = 3.027 \pm 8 \cdot 10^{-5}$ for blue curve. More comments on the measurement of $f(a_w)$ will be discussed in the following chapter. As can be seen the red curve approximates data in the best way for small values of a_w (smaller figure inside) but fails to approximate the function for $a_w > 0.4$ (as the fit was done just for range (0,0.3)). The blue curve behaves in the opposite way.

2. Description of experiments

2.1 PEM fuel cells

The first usable fuel cell was developed by Thomas Francis Bacon in 1932 ([16]), with an output power of 5 kW. However, it was an alkaline fuel cell where an aqueous solution of KOH was used as the electrolyte. PEM fuel cell was invented in the early 1960s by Willard Thomas Grubb and Leonard Niedrach ([16]), but the Nafion membrane was used as an electrolyte in 1966 for the first time. Nowadays, PEM fuel cells are the best candidate for vehicles and other mobile applications due to their compactness compared to other types of fuel cells.

In this section, we will explain how the PEM fuel cell works. The scheme of the PEM fuel cell is shown in picture 2.1. The anode is fed with hydrogen,

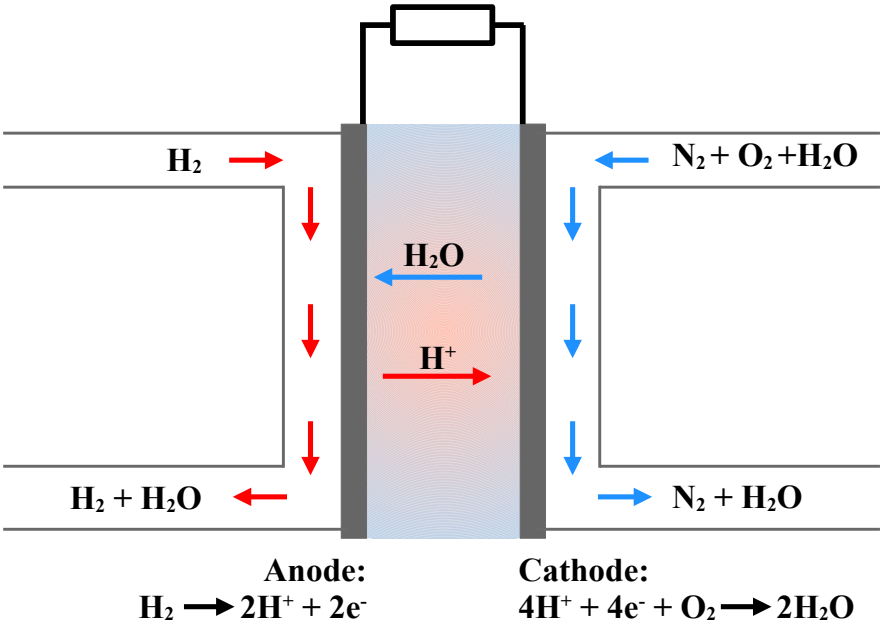

Figure 2.1: The picture shows the scheme for the PEM fuel cell. The hydrogen is fed to the anode, which is made from platinum. On the anode (left), the hydrogen oxidation reaction (HOR) proceeds due to the presence of platinum, which is the best-known catalyst for the HOR reaction. After splitting the hydrogen, the H^+ ions (protons) move through to membrane to the cathode. The cathode is fed with air, consisting mainly of nitrogen, oxygen, and water vapor. Protons, electrons, and oxygen react together and form water on the cathode. Water is firstly carried away by the flow of nitrogen and some residual not used oxygen, and secondly transported through the membrane by diffusion (as there is no water on the other side of the membrane, the water concentration gradient pushes water through the membrane.)

and the cathode is fed with air. On the anode, the HOR reaction proceeds, and

protons are transported through the membrane to the cathode, and electrons are transported through the external electric circuit to the cathode. The chemical reactions and transport of both charged species (protons and electrons) is driven by the overpotential of the chemical reaction. Using the equation 1.86, we can write down the overpotential for fuel cell as described on the picture 2.1. It holds that

$$\eta_{HOR} = \frac{1}{2F}\left(\tilde{\mu}_{H_2} - 2\tilde{\mu}_{H^+} - 2\tilde{\mu}_{e^-}\right) \tag{2.1}$$

$$\eta_{ORR} = \frac{1}{4F}\left(2\tilde{\mu}_{H_2O} - 4\tilde{\mu}_{H^+} - 4\tilde{\mu}_{e^-} - \tilde{\mu}_{O_2}\right). \tag{2.2}$$

If we assume that we are at standard atmospheric pressure and room temperature and use the fact that chemical potentials of formation of pure species such as hydrogen and oxygen are set to be zero, we can rewrite 2.1 and 2.2 as

$$\eta_{HOR} = -\frac{1}{F}\left(\tilde{\mu}_{H^+} + \tilde{\mu}_{e^-}\right) \tag{2.3}$$

$$\eta_{ORR} = \frac{1}{F}\left(\frac{1}{2}\tilde{\mu}_{H_2O} - \tilde{\mu}_{H^+} - \tilde{\mu}_{e^-}\right). \tag{2.4}$$

The production of protons (which is given by Butler-Volmer equations 1.87) must be the same on both sides. However, the production on the right must have the opposite (negative) sign, as protons are consumed (not produced) by HRR on the right electrode. Therefore, if we assume both overpotentials to be that small, then we can approximate $\sinh(x) \approx x$, and get

$$j_0^{HOR}\,\eta_{HOR} = -j_0^{ORR}\,\eta_{ORR}, \tag{2.5}$$

where equality holds if both electrodes are identical (In the case where different electrodes were used on both sides, the characteristics of the electrodes would change the equation). Now let us assume that the fuel cell has an open external circuit. Therefore, the production of protons and consequently water production is zero. As the reactions are not in progress, both overpotentials 2.3 and 2.4 are zero. By comparing both expressions, we get

$$\frac{1}{2}\tilde{\mu}_{H_2O} - \tilde{\mu}_{H^+}|_{right} - \tilde{\mu}_{e^-}|_{right} = -\tilde{\mu}_{H^+}|_{left} - \tilde{\mu}_{e^-}|_{left} \tag{2.6}$$

$$\tilde{\mu}_{H_2O} = 2\left(\Delta\tilde{\mu}_{H^+} + \Delta\tilde{\mu}_{e^-}\right), \tag{2.7}$$

where $\Delta\tilde{\mu}$ denotes the difference between electrochemical potential on the right-hand side and the left-hand side. The value of $\tilde{\mu}_{H_2O}$ is $-237.18\,\mathrm{kJ/mol}$ for formation of liquid water ([14]). As protons are not moving through the membrane. The electrochemical potential of protons inside the membrane must be constant, which means $\Delta\tilde{\mu}_{H^+} = 0$. The difference in electrochemical potentials of electrons between the right and left electrode is UF. In the case of an open circuit, we have $U = U_{OCV}$, where OCV stands for *Open Circuit Voltage*. From 2.7 we have

$$U_{OCV} = -\frac{\tilde{\mu}_{H_2O}}{2F} \approx 1.23V. \tag{2.8}$$

As $\eta_{HOR} = 0$ we have $\tilde{\mu}_{H^+}|_{left} = -\tilde{\mu}_{e^-}|_{left}$. Without loss of generality, we can set the electrochemical potential of electrons on the left to be zero. This immediately

gives us $\tilde{\mu}_{H^+}|_{left} = 0$ That is shown in picture 2.2 with a blue line. Inside the membrane, the blue line shows the electrochemical potential of protons, and outside the membrane, it shows the electrochemical potential of electrons. The difference between the electrochemical potential of electrons on electrodes is the voltage (in this case, $U = U_{OCV}$).

After closing the electrical circuit, the protons start to move from the left to the right through the membrane. That means that $\tilde{\mu}_{H^+}$ must decrease from left to right in the membrane. Moreover, as the proton flux is now positive (from left to right), the overpotential $\eta_{HOR} > 0$. As $\tilde{\mu}_{e^-}|_{left} = 0$, $\tilde{\mu}_{H^+}|_{left}$ must be negative. Now we want to show how the voltage will change after closing the circuit. Plugging 2.3 and 2.4 into 2.5 we get

$$\frac{j_0^{HOR}}{j_0^{ORR}}\eta_{HOR} = -\eta_{ORR} \tag{2.9}$$

$$-\frac{j_0^{HOR}}{j_0^{ORR}}\frac{1}{F}\tilde{\mu}_{H^+}|_{left} = -\frac{1}{F}\left(\frac{1}{2}\tilde{\mu}_{H_2O} - \tilde{\mu}_{H^+}|_{right} - \tilde{\mu}_{e^-}|_{right}\right) \tag{2.10}$$

$$-\frac{j_0^{HOR}}{j_0^{ORR}}\frac{1}{F}\tilde{\mu}_{H^+}|_{left} = \frac{\tilde{\mu}_{H^+}|_{right}}{F} + U_{OCV} - U \tag{2.11}$$

$$U = U_{OCV} + \frac{j_0^{HOR}}{j_0^{ORR}}\frac{1}{F}\tilde{\mu}_{H^+}|_{left} + \frac{\tilde{\mu}_{H^+}|_{right}}{F}. \tag{2.12}$$

The second and the third term on the right-hand side of 2.12 are both negative. (Second term is negative, as explained before, and the third term must be smaller than the second, as $\tilde{\mu}_{H^+}$ decreases in the membrane.) Therefore, we see that the measured voltage is always smaller than the U_{OCV}. The function of potential for a closed circuit is shown on picture 2.2 with red lines. Inside the membrane, the electrochemical potential of protons is shown, and on the electrodes, the electrochemical potential of electrons is shown.

2.2 Experimental setup of hydrogen pump

The goal of this thesis is to describe experimental results measured by J. Benziger et al. in 2015, published in [1]. In the article, proton and water flux through the Nafion membrane were measured; however, no theoretical explanation for the data was given. This chapter will describe the experimental setup and comment on the measured data.

As mentioned earlier, to do experiments as simple as possible (to avoid having a lot of unknown parameters), the water and proton transport inside the PEM membrane was studied not on fuel cell but the so-called "hydrogen pump." The scheme of the setup in co-current operation is shown in Figure 2.3

U was set to negative on the left electrode for counter-current operation. That causes the change of sign of the overpotentials 1.98 and 1.99 on the left and right electrode. Because of that, the role of anode and cathode was switched (see 2.4)

2.3 Experimental results for Hydrogen pump

The water and proton flux through the hydrogen pump were measured for Different applied voltages. The relative humidity of the left electrode feed was set to

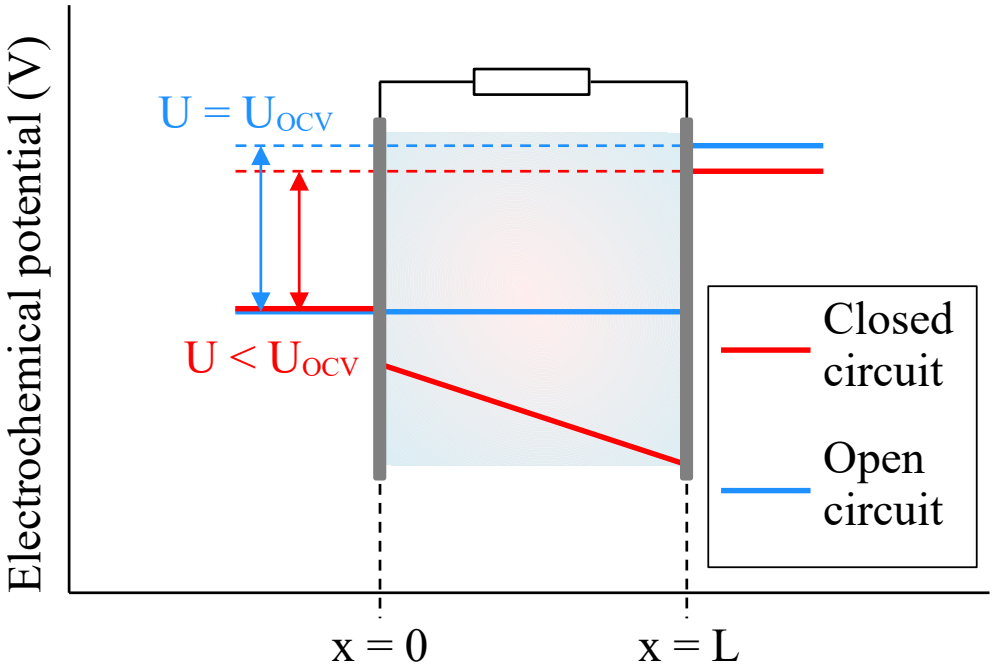

Figure 2.2: The figure shows the profile of electrochemical potential in the hydrogen pump. At the open circuit, the difference in electrochemical potential of electrons is equal to the open-circuit voltage. At a closed circuit, the protons start to move, which is caused by the decrease of the electrochemical potential of protons inside the membrane (note that the although in the figure the profile of electrochemical potential inside the membrane is linear, this is not true in general and the picture is just for illustration). However, the electrochemical potential of electrons on the right electrode is lower than at the open circuit, which means that the voltage of FC is always lower than the OCV.

30% 50% and 70 % in the experiments. The temperature was set to a constant value and did not change during each measurement. After setting an electric potential value, it took some time to equilibrate the system. After equilibration of the system (the proton flux and water flux started to be constant), the measurements were made. After that, a new value of the voltage was set. The voltage was altered from -1.0V to 1.0V with a step of size 0.03V for smaller Voltages (in absolute value) and with step size 0.1V for higher Voltages. The measured data can be seen in 2.5

For lower applied voltages, the proton flux increases linearly with increasing voltage. However, for voltages $U > 0.2$V and $U < -0.2$V, the flux cease to be linear and saturates at specific values. The more humidified the left electrode feed is, the higher the saturation current is (in absolute value). In [1] the author tried to explain the measured data using a simple model, where the membrane was approximated by a single point ($0D$ model). They use the same CIT model equations in the shape 1.68 and 1.69, but due to the $0D$ model, all L_{ij} coefficients are constants, and the gradients of μ_w (or water activity a_w) and ϕ are approximated as $\nabla\mu_w \approx (\mu_w|_{x=L} - \mu_w|_{x=0})/t_{mem}$ and $\nabla\phi \approx (\phi|_{x=L} - \phi|_{x=0})/t_{mem}$ where

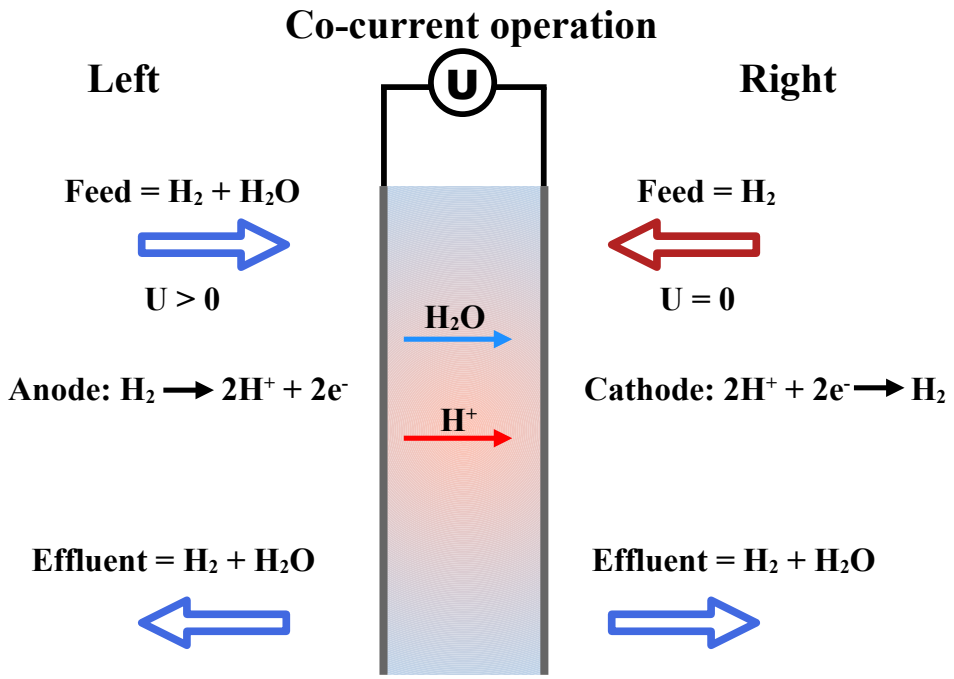

Figure 2.3: The picture shows the co-current operation of the hydrogen pump (Nafion membrane – colorful, sandwiched between two platinum electrodes-grey). Co-current means that water and protons are transported through the membrane in the same direction. That is achieved for $U > 0$ on the left electrode. (Without loss of generality, U is always set to be 0 on the right electrode) Voltage decreases in the membrane from left to right. Lorentz's electric force makes protons move to the lower electric potential. That causes the flux of protons from left to right. Water firstly moves to the right due to diffusion (as on the left side we have non-zero diffusivity and on the right side we do not) and secondly due to electro-osmotic drag.

t_{mem} is the thickness of the membrane. However, this model can not explain the current saturation.

2.4 Measurements of phenomenological coefficients

The water diffusivity and concentration as a function of water activity in Nafion 115 were measured experimentally in [17] and [15] respectively. In [17] the measurement of proton conductivity is also presented. However, the technique used to recover the conductivity dependence on water activity was based on incorrect assumptions, which will be discussed later. The goal of this section is to introduce the measurements techniques shortly and, using the measurements, determine the value of the coefficient L_{dif} and the functional dependence $f(a_w)$ which is the same for the product of D_w and c_w and also for proton conductivity σ_p as follows from arguments presented in 1.3.2.

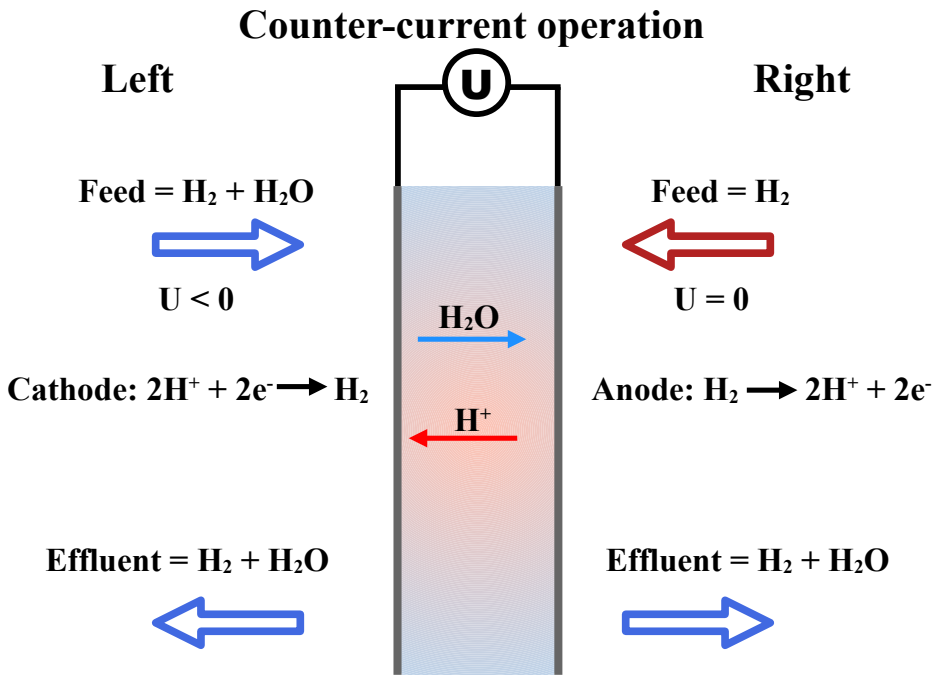

Figure 2.4: The picture shows the hydrogen pump (Nafion membrane – colorful, is sandwiched between two platinum electrodes-grey) in counter-current operation. Counter-current means, that protons are transported through the membrane in the opposite direction as water. That is achieved for $U < 0$ on the left electrode. (Without loss of generality, U is always set to be 0 on the right electrode) Voltage decreases in the membrane from right to left. Lorentz's electric force makes protons move to the lower electric potential. That causes the flux of protons from right to left. Water moves to the right due to diffusion, but the proton flux in the opposite direction slows down the water flux.

The measurements of water self-diffusivity were made using the *pulsed gradient spin echo NMR* method for different water activities and temperatures. The effective diffusion coefficient as a function of water activity and the temperature was fitted as ([17])

$$D_w = 0.265\mathrm{e}^{\frac{-3343}{T}} a_w^2 \mathrm{cm}^2/\mathrm{s} \tag{2.13}$$

The water concentration measurements were made as an absorption experiment, where the membrane was immersed in an environment with constant relative humidity, and the water content in the membrane was measured as a function of time. A classical irreversible thermodynamic model was used to express the water flux through the membrane interface as a function of c_w and D_w

$$j_w = -D_w c_w \frac{1}{a_w} \nabla a_w \tag{2.14}$$

with the same boundary conditions for water flux as presented in 1.4.3. For D_w the expression 2.13 was used. A handful of expressions for concentration as a function of water activity were derived. In general, all of them had good agreement with experimentally measured data. However, they chose the *GAB*

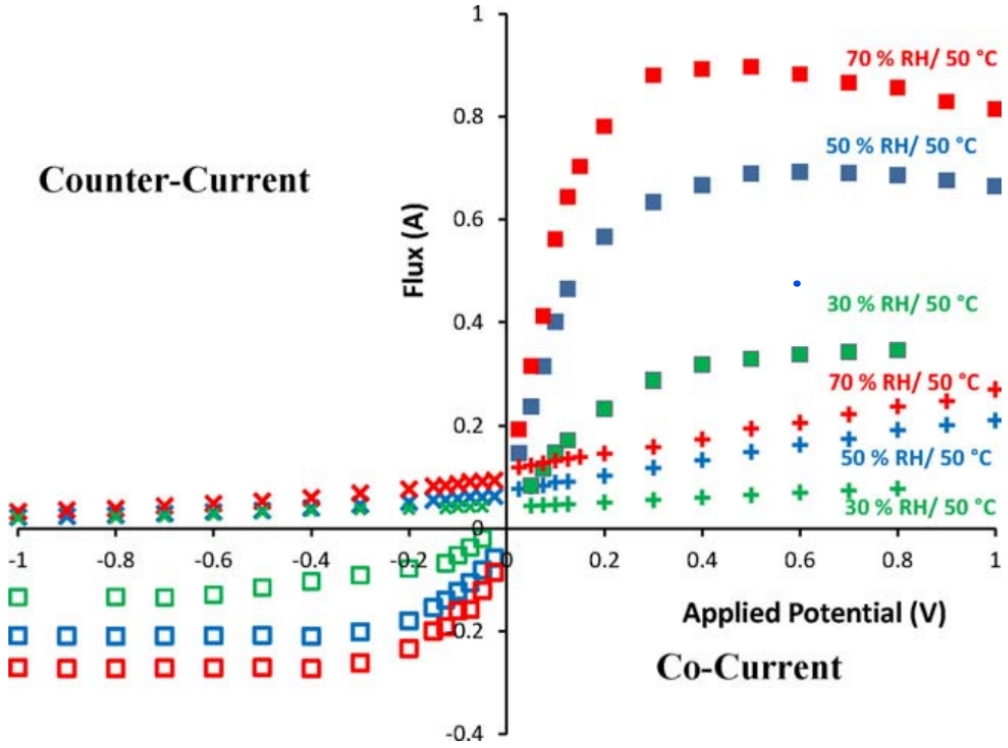

Figure 2.5: The figure taken from [1] shows the measured data for proton and water flux as a function of applied potential. The crosses × and + correspond to the water flux, and squares correspond to the proton flux (solid squared for the co-current operation and hollow squares for counter-current operation). All data corresponds to the measurement for 50 °C. Green, blue and red data correspond to left electrode feed humidity of 30%, 50%, and 70% respectively.

isotherm model given as

$$c_w(a_w) = \frac{\rho_N}{EW} \frac{\lambda_G c_G k_G a_w}{(1 - k_G a_w)(1 + (c_G - 1)k_G a_w)}, \tag{2.15}$$

and the reason is described in Section 4 of [15]. The parameters λ_G, c_G and k_G were fitted to be $\lambda_G \approx 1.93$, $c_G \approx 44.3$ and $k_G \approx 0.9$. EW and ρ_N stands for equivalent weight (weight of Nafion polymer per 1 mol of SO_3 groups) and ρ_N is the density of the membrane in a dry state. From [18] we have $\rho_N = 2120\mathrm{kg\,m^{-3}}$ and from [19] we have $EW = 1.11\mathrm{kg\,mol^{-1}}$.

Combining the equations 2.15 and 2.13 we get

$$L_{dif} f(a_w) = \frac{\rho_N}{EW} \frac{0.265\mathrm{e}^{\frac{-3343}{T}} \lambda_G c_G k_G a_w^3}{(a - k_G a_w)(1 + (c_G - 1)k_G a_w)}. \tag{2.16}$$

Now we can choose the constant L_{dif} arbitrarily. We decided to put

$$L_{dif} = 0.265\mathrm{e}^{\frac{-3343}{T}} \tag{2.17}$$

$$f(a_w) = \frac{\rho_N}{EW} \frac{\lambda_G c_G k_G a_w^3}{(1 - k_G a_w)(1 + (c_G - 1)k_G a_w)}, \tag{2.18}$$

as it is advantageous for the code to choose it in that way. The other coefficients (ξ and σ_p^0) will be determined from the simulations. It will also be shown that

the measurement of $\sigma_p(a_w)$ can not be done as a resistance measurement of the Nafion membrane for various humidities of the membrane surroundings (as in [17]). It will also be shown why the drag coefficient measurements, as a ratio of j_w and j_p for zero X_w, can not give correct results.

The last couple of coefficients, that can be measured experimentally are j_0 and k_w from boundary conditions 1.100, 1.101 and 1.104, 1.105 respectively. The value of j_0 is not constant for given reaction, because it also depends on the surface properties of the electrode. According to [20], j_0 can be written as

$$j_0 = j_0^{HOR} a_C L_C, \tag{2.19}$$

where $a_C = 1000\text{cm}^2/\text{mgPt}$, $L_C = 0.5\text{mgPt/cm}^2$ and $j_0^{HOR} = 7.21 \cdot 10^{-3}\text{A/cm}^2$ are again taken from [20]. The value of k_w can be taken from [15] and is $k_w = 3.2 \cdot 10^{-6}\text{mol cm}^{-2}\text{s}^{-1}$. However, its value for temperature $T = 50°\text{C}$ was only estimated, and it is strongly temperature dependent (for comparison, at $T = 70°\text{C}$ the measured value of k_w is $3.5 \cdot 10^{-7}\text{mol cm}^{-2}\text{s}^{-1}$). Due to this fact, this value was considered to be a parameter of our model, and as we will see, different value (although of the same order) fits better for the model and the data.

In this chapter, we presented the measurements of Jay Benziger's group [8] introduced in [1]. The measured data could not be explained using the simple zero-dimensional model, and therefore, we will use a one-dimensional model. Later we explained the measurements of phenomenological coefficients and their dependence on the water activity and the other coefficients from our model.

3. Numerical implementation

The numerical implementation of the equation 1.83 with boundary terms 1.100, 1.101 and the equation 1.84 with boundary terms 1.104 and 1.104 is done by using *Finite Volume method* (FVM). The method is explained in appendix A and was implemented in Julia library *VoronoiFVM*. For implementation, we must specify the grid, the flux, and boundary conditions, represented by the boundary reaction term. Detailed documentation is available on VoronoiFVM website [21].

The grid was chosen in such a way that the domain was divided into 500 control volumes, and the first and the last were then again divided into 500 smaller control volumes. That led to the domain being divided into 1498 control volumes, where the first 500 and the last 500 were 500-times smaller than the rest. This construction was done because both searched functions a_w and ϕ were changing dramatically near the electrodes, and the numerical solution depended on the grid. For a number of control volumes in the order of hundreds or few thousands before the grid refinement on the boundaries was made. Although the same results could be achieved for slightly smaller refinement of first and last control volume, higher refinement (the mentioned 500) was kept, as it did not have a significant impact on computation speed (as one solution of the system for given boundary conditions lasted less than one second).

The numerical approximation of flux was given by simple approximation of the derivatives as the difference of the function value in the neighboring volumes. In *VoronoiFVM* the *flux* function is a function that computes the flux between the neighboring volumes for a given pair of control volumes A and B (see the notation of control volumes, grid points, and faces introduced in A.1). The numerical approximation of 1.83 and 1.84 between two control volumes A and B is then

$$j_p(f_{AB}) \approx -\sigma_p^0 \mathcal{F}(a_w(f_{AB})) \left(\frac{\nabla\phi(f_{AB})}{F} + \frac{RT\xi}{F^2} \frac{\nabla a_w(f_{AB})}{a_w(f_{AB})} \right) \tag{3.1}$$

$$j_w(f_{AB}) \approx j_p(f_{AB})\xi - L_{dif}\, \mathcal{F}(a_w(f_{AB})) \frac{\nabla a_w(f_{AB})}{a_w(f_{AB})} \tag{3.2}$$

where f_{AB} is the face between the control volumes A and B. The function $\mathcal{F}(a_w)$ is the functional dependence of phenomenological coefficients on a_w from 2.18, where $\mathcal{F}$ was used instead of f just to avoid the similarity of notation with faces. The derivatives were approximated as

$$\nabla\phi \approx \frac{\phi(b) - \phi(a)}{h} \tag{3.3}$$

$$\nabla a_w \approx \frac{a_w(b) - a_w(a)}{h} \tag{3.4}$$

where a and b are the nodes inside the volumes A and B, and h is the distance between a and b. The *VoronoiFVM* always computes h for the specific pair of nodes, and therefore, in the code h is omitted from equations 3.3 and 3.4. As water activity has its values well defined just inside the control volumes, we had to define them on the face, which was done as an average of the values inside the volumes, that share the respective face.

$$a_w(f_{AB}) \approx \frac{a_w(b) + a_w(a)}{2} \tag{3.5}$$

Flux on the boundary was prescribed by using the *breaction* function. This function is used when there is some chemical reaction on the boundary, and the flux is given by the reaction rate, which depends on the values of the solution in the edge nodes of the network. Therefore, equations 1.104 and 1.105 were used explicitly as *breaction* terms for water flux, and equations 1.100 and 1.101 were used explicitly as *breaction* terms for proton flux. As the experiment was measured under constant temperature and atmospheric pressure, the only parameters that were changing were relative humidities of the hydrogen on both sides of the hydrogen pump ($RH|_{x=0^-}$, $RH|_{x=L^+}$) and the applied voltage (U).

As the numerically achieved solutions for water activity $a_w(x)$ has a very steep derivative near the electrode for some values of U, it could happen that the water activity computed on the face between the first and second control volume (or between last and last but one) using 3.5 was just slightly bigger than zero. However, the slope of $a_w(x)$ causes, that $a_w(0)$ (water activity in the first node) happened to be negative. To avoid this numerical artifact, we rewrite the equations by using new function $\nu(x)$ instead of $a_w(x)$ where

$$a_w(x) = \mathrm{e}^{\nu(x)}. \tag{3.6}$$

Thanks to that, for an arbitrary value of ν, the water activity must remain greater than zero[1]. It also changed the term with the ∇a_w as the original term with $\nabla \mu_w$ can be rewritten as

$$\nabla \mu_w = \nabla \left(\mu_w^0 + RT\nu \right) = RT \nabla \nu, \tag{3.7}$$

where we used the definition of the chemical potential of water 1.51. That can be numerically approximated simply as the difference of the values of ν in neighboring control volumes.

Besides that, for some values of U, very small values of a_w occurred. Then, the function $f(a_w) \propto a_w^2$ was numerically a zero. That caused the resulting fluxes to be also zero. To avoid that, we added a small constant 10^{-2} to $\mathcal{F}(a_w)$. Although this addition of a constant was only made to solve a numerical problem, it also has physical meaning. Before the constant was added, for a dry membrane ($a_w = 0$), the electric conductivity was zero (electric resistance was infinite), and diffusivity was also zero (this means that after inserting one water molecule inside the membrane, the molecule would not move). The addition of a constant is a simple way to deal with these paradoxes.

After these two changes, the numerical implementation of equations inside the membrane is

$$j_p(f_{AB}) \approx -\sigma_p^0 \left(\mathcal{F}(\mathrm{e}^{\nu(f_{AB})}) + 10^{-2} \right) \left(\frac{\nabla \phi(f_{AB})}{F} + \frac{RT\xi}{F^2} \nabla \nu(f_{AB}) \right) \tag{3.8}$$

$$j_w(f_{AB}) \approx j_p(f_{AB})\xi - L_{dif} \left(\mathcal{F}(\mathrm{e}^{\nu(f_{AB})}) + 10^{-2} \right) \nabla \nu(f_{AB}) \tag{3.9}$$

and the equations for water flux on the boundary change to

$$j_w|_{x=0} = k_w(\mathrm{e}^{\nu(0)} - RH|_{x=0^-}) \tag{3.10}$$

$$j_w|_{x=L} = k_w(RH|_{x=L^+} - \mathrm{e}^{\nu(L)}), \tag{3.11}$$

[1] If the water activity will exceed the value 1, which means that the water could condensate and form a liquid water drops. In such a case, our model can not be used.

where 0 and L are the coordinates of the first and the last node.

VoronoiFVM solves equations iteratively. We were using the newton method in our program. Such a method needs some initial guess from which the iterations will start. For a simple problem (for instance, our problem for $U = 0$), some reasonable vector of the same constant is sufficient to achieve convergence. However, for some higher U, our problem had problem to converge with a constant initial guess of solution. What we did to help the convergence was that initially, we solved the problem for $U = 0$, and then we used the solution as the initial guess for computing the solution for slightly bigger U. The new solution was then again used as an initial guess for the following problem with higher U. If we wanted to do calculations in the interval from -1V to 1V, two separate cycles were needed, one from 0 to 1 and another from 0 to -1. The voltage difference between two subsequent computations was 0.005V.

In this chapter, we introduced the numerical implementation of our hydrogen pump model in Julia programming language using the library *VoronoiFVM*. We also introduced how we dealt with convergence problems numerically. Note that convergence problems appear because the solution itself can have an arbitrarily large derivative (as we have shown in Section 1.5) and not due to a wrongly chosen method or some other numerical problem.

4. Results

4.1 Explanation of hydrogen pump data

This chapter will present the results of simulations of water and proton flux inside the hydrogen pump. At first, we will try to find the parameters σ_p^0, k_w, and ξ such that the results of the model will approximate the experimental data from [1] shown in Figure 2.5. It was not convenient to use any fitting method, as for some values of parameters, the computations would not converge. Therefore, we were setting the parameters by hand until the model fitted the data in the best possible way. The model, in comparison with measured data for the 50 % relative humidity of the left electrode feed, can be seen in Figure 4.1.

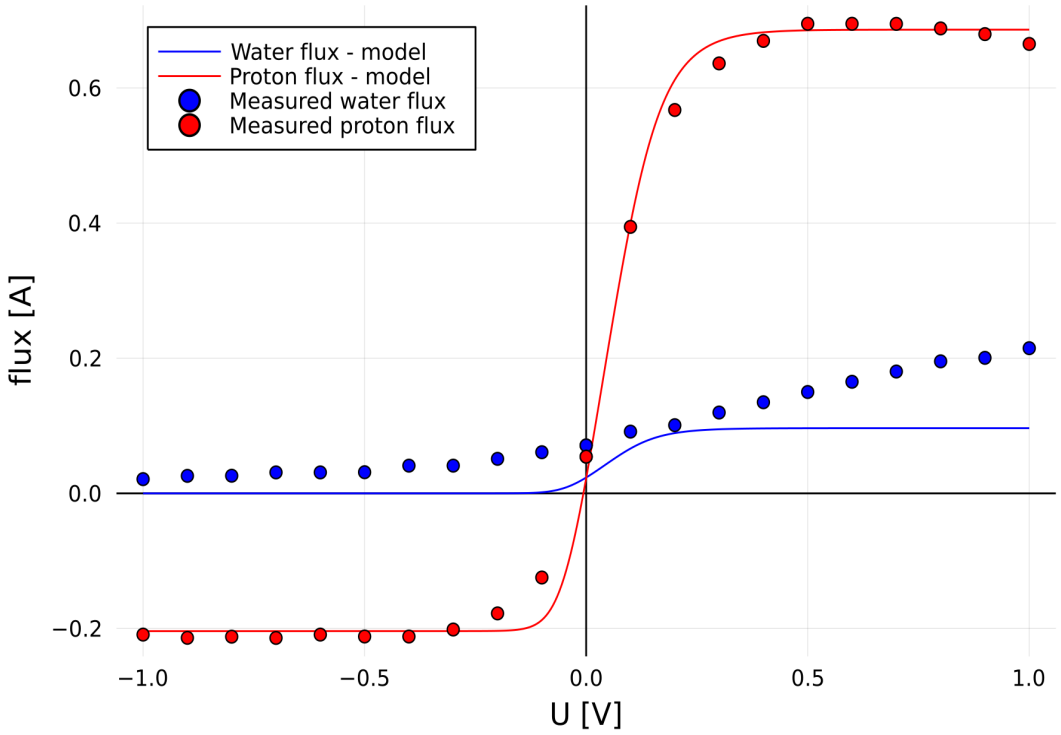

Figure 4.1: The water flux is blue (line for the model, circles for experimental data), and the proton flux is red (line for the model, circles for experimental data). As can be seen, the constant was fitted, so that proton flux is relatively well approximated. In the region where the approximation is the worst (where the growth passes to the plateau), the experimental data has the most significant errors (as can be seen on very similar measurement from [17] page 108). However, the approximation of water flux is wrong. The reasons why the model behaves that way and how can be changed will be discussed later.

The value of fitted drag coefficient, k_w and σ_0^p are $\xi = (0.20 \pm 0.01)$, $k_w = (2.0 \pm 0.05) \cdot 10^{-2} \mathrm{mol\,m^{-2}s^{-1}}$ and $\sigma_0^p = (2.15 \pm 0.15) \cdot 10^{-2}\,\mathrm{S/m}$. However, the value of sigma itself does not give us much information, as it has to be multiplied with the $f(a_w)$. We will compare fitted dependence for σ_p with the AC measured dependence from [17] from page 107. The comparison can be seen in figure 4.2.

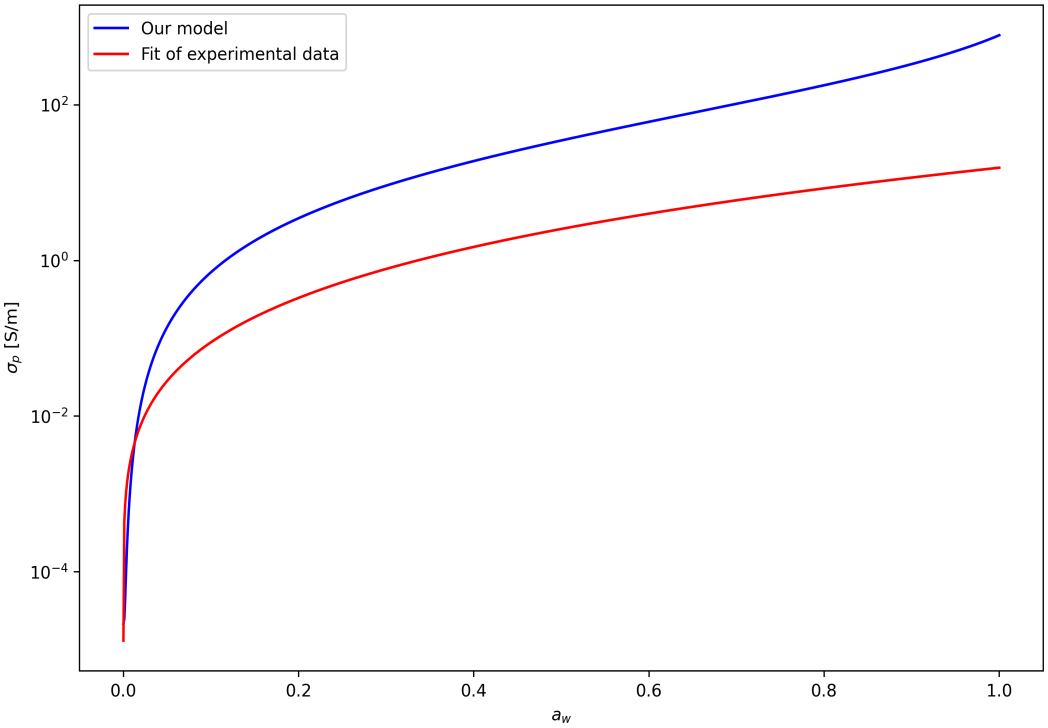

Figure 4.2: The figure shows how our model of the membrane conductivity differs from the fitted experimental data. The experimentally measured data shows that the conductivity is approximately ten times lower than according to our model. It is because the protons moving through the membrane interact with the water molecules, creating the dry spot near the electrode. A more detailed explanation will be given later.

To understand the behavior of the membrane, we must shortly explain how the transport processes inside the membrane works. The transport of water is realized in two ways. The first is the diffusion, where water moves in the opposite direction as the concentration gradient, and the second is via electro-osmotic drag. Electro-osmotic drag causes protons to move through the membrane, interact with water, and pull the water molecules in the same direction as protons' movement. That also works in the opposite way, which causes non-zero proton flux, even if the applied voltage is zero, as the protons are pulled through the membrane with the water in the direction opposite to the concentration gradient. Besides, protons are transported due to an electric potential gradient (as they have an electric charge). More detailed mechanisms of transport of protons due to electric field gradient inside the PEM membrane can be found in [22]. In the Figure 4.3, we can see what is the influence of individual mechanisms on water flux. For zero applied potential $U = 0$, we see that as the humidity on the left electrode is 50%, and on the right electrode it is 0%, the water activity continuously decreases inside the membrane, which is the expected behavior. Note that the reason why the water activity on the left is slightly under 0.4 and not 0.5 is that we have non-zero water flux, which is proportional to the difference between water activity on the boundary and relative humidity of the electrode feed. However, for slightly higher voltage, the profile of water activity starts to have an opposite gradient,

which means that (together with the fact that water flux is positive, which can be seen in figure 4.1) water flux due to electro-osmotic drag is higher than due to diffusion, which has the opposite direction now. As with the rising U, the

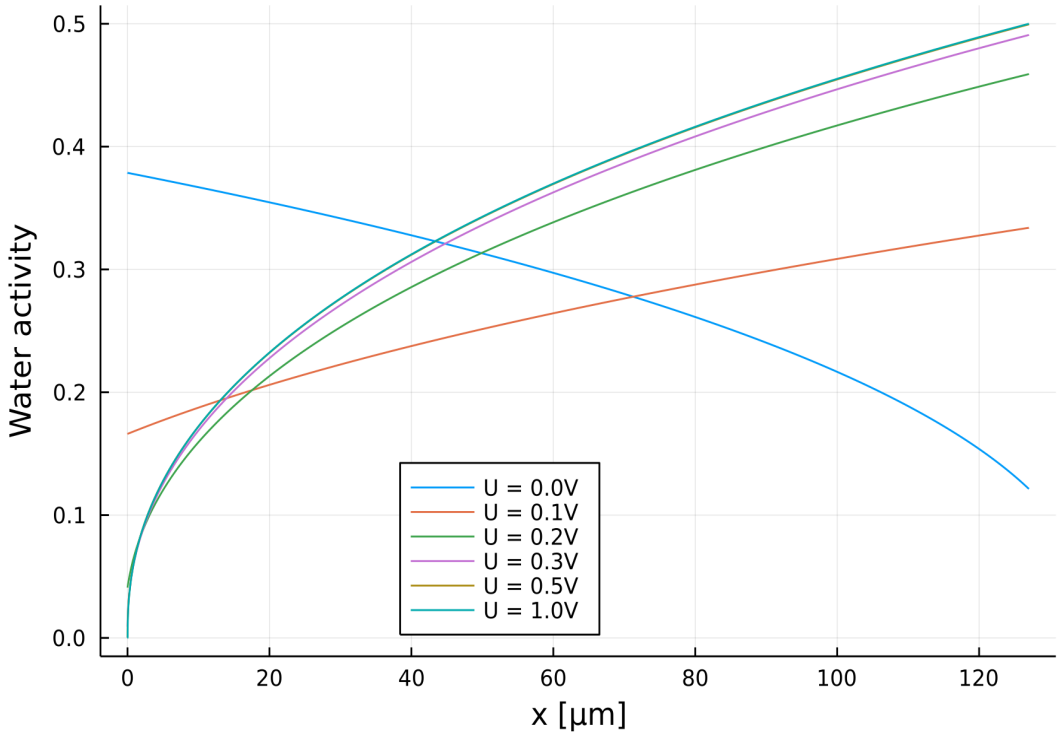

Figure 4.3: This figure shows the profiles of water activity inside the membrane. It can be seen that as the voltage increases, moving protons begin to entrain the water molecules, which causes the water activity drops.

proton flux water flux rises. It must respect the boundary conditions, and the difference between RH on the electrode and water activity on the boundary on the membrane must increase. That can be seen in Figure 4.3 as the voltage is increasing. For voltages 0.3 V and higher, the water activity at the boundary drops nearly to zero. That results in a massive decrease of proton conductivity (as can be seen in figure 4.2), and consequently to the saturation of water flux and proton flux.

The fact that rising the voltage does not increase the proton flux can also be seen from the point of view of how the course of electrochemical potential in the membrane changes. In Figure 4.4, the course of the electrochemical potential of protons in the membrane can be seen. We see that for values greater than 0.2V, the course of electrochemical potential in most of the membrane remains unchanged. Consequently, the dominant driving force of the proton and water movement – gradient of the electrochemical potential protons remains unchanged. That also explains that both fluxes are constant for higher applied voltages. However, the higher voltage causes a much steeper gradient near the left electrode, which is needed to compensate the rapid conductivity drop due to a dry spot near the membrane. We can say that increasing the voltage only makes the gradient near the electrode steeper and simultaneously dries a membrane a little more.

The main goal of Figure 4.4 is to demonstrate that the profile of electrochem-

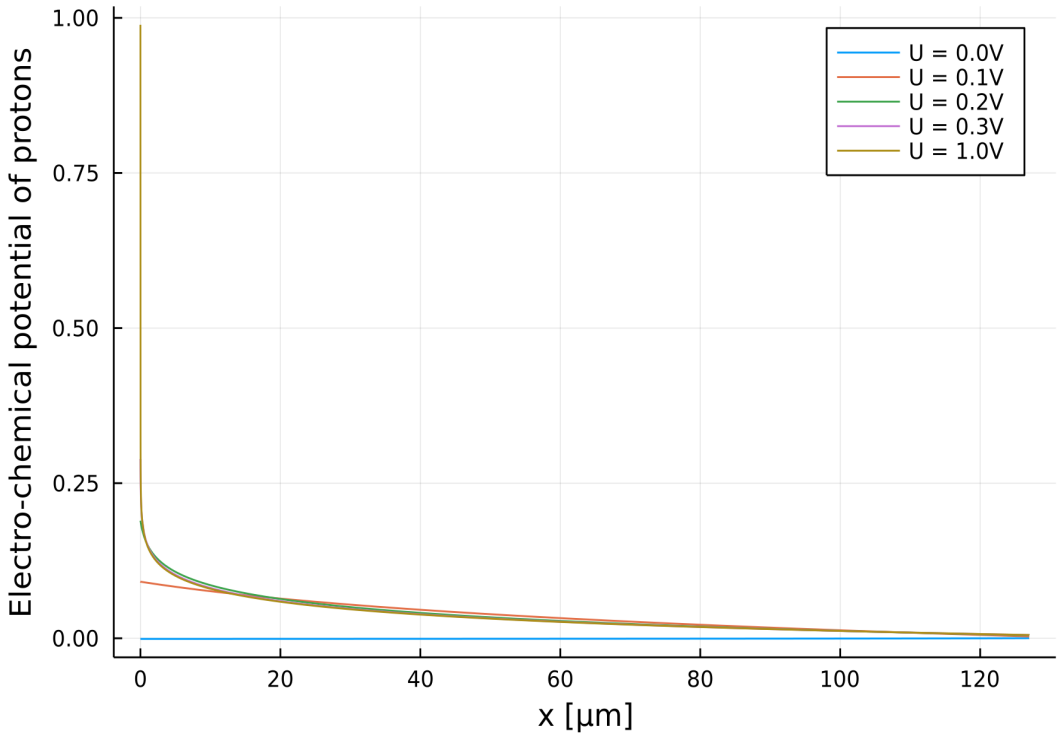

Figure 4.4: The figure shows the course of the electrochemical potential of protons inside the membrane. For zero voltage, the electrochemical potential is identically zero, and water transport is caused only by diffusion. The transport of protons is only due to electro-osmotic drag, as protons are pulled by water molecules. For higher voltages, the potential decreases from left to right. However, for $U > 0.2$V, the curves look basically the same up to the region very close to the left electrode (boundary). The higher the voltage is, the greater is the gradient near the boundary in order to compensate dry spot with very low proton conductivity.

ical potential looks the same for higher voltages ($U > 0.2$V). However, we can not see what is happening near the left electrode. For this purpose we plotted the same data as in 4.4 to another figure 4.5 as a log-log plot. In 4.5 the behavior in the first μm on the membrane can be seen very well. It is obvious that the value of electrochemical potential near the boundary is different for every value of U.

However, the voltages $U = 0.5\,\mathrm{V}$ and $U = 1.0\,\mathrm{V}$ and respective curves shows unnatural behaviour. Together with the fact that although we could find the values of σ_p^0, k_w and ξ such that the proton flux was approximated well, we could not approximate the water flux well enough and some other facts that will be presented in the following section, this gives us reason to believe that the presented CIT model is not enough to explain the measured data in its full complexity.

4.2 Model inconsistency with experiments

In the previous section, we summarised the results of the CIT model for boundary conditions for water. We also presented the problem with the water flux, which saturates at the same time as the proton flux, and the reason for both is the same

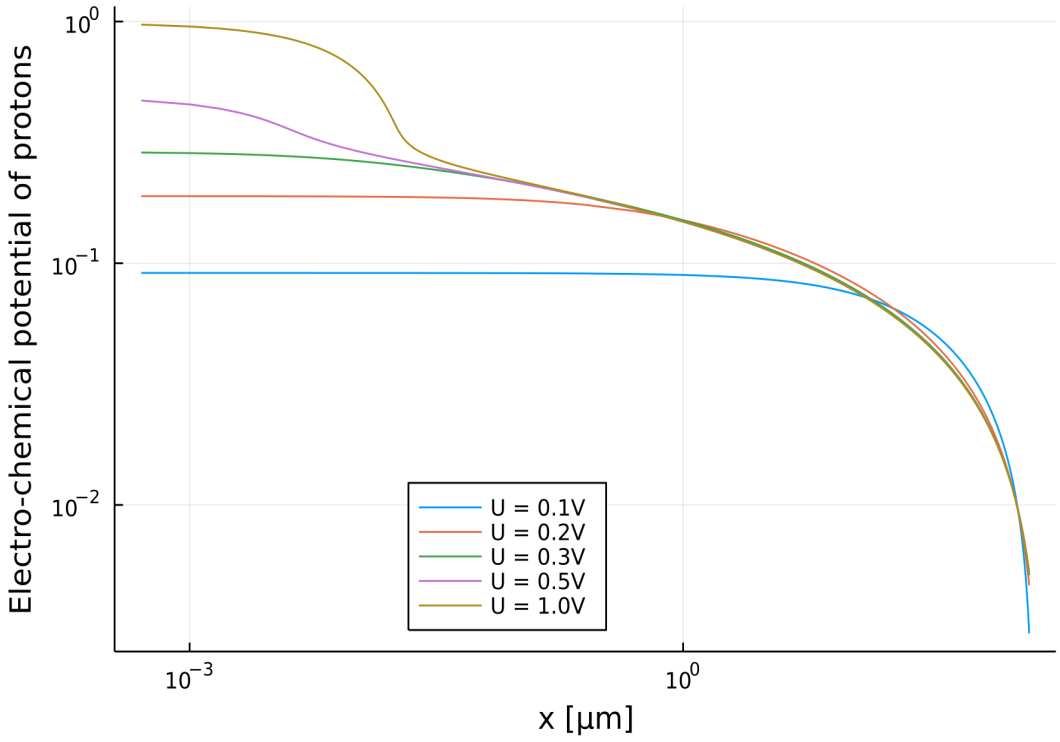

Figure 4.5: The figure shows the same data as in 4.4. In this figure, both axes are logarithmic, which allows us better insight into what is happening near the boundary of the membrane.

– the dry spot near the left boundary on the membrane. Therefore, according to the model, the water flux must saturate at the same time as the proton flux, which contradicts the experimental results.

The second inconsistency is that although fitted values for phenomenological coefficients must hold for different boundary conditions, they do not. If we set the humidities to be $RH|_{left} = 30\%$ and $RH|_{right} = 0\%$ and for another simulation $RH|_{left} = 70\%$ and $RH|_{right} = 0\%$, we did not get the agreement with the experimental data as can be seen from figures 4.6 and 4.7. The possible explanation for the inconsistencies is that our model of the hydrogen pump is not complete. It consists of three parts. The first part are equations for the membrane, the second part are equations for the water flux on the boundary, and the third part are the equations for proton flux on the boundary. We will further assume that the problem that causes water transport saturation is the same that causes, that model proton fluxes do not match with experimental data. We will formulate the issue as follows: *Experimental data show us that after proton flux saturates, water flux still rises. The observation of our model tells us that water flux saturation and proton flux saturation are both the consequence of dry spots in the membrane. Assuming only the equations in the membrane, is it possible that for constant j_p, the j_w will grow with increasing the voltage?* Or, more formally, can

$$\left(\frac{\partial j_w}{\partial X_p}\right)_{j_p=const.} > 0 \; ? \tag{4.1}$$

To calculate whether 4.1 can be positive, we need to have j_w as a function of

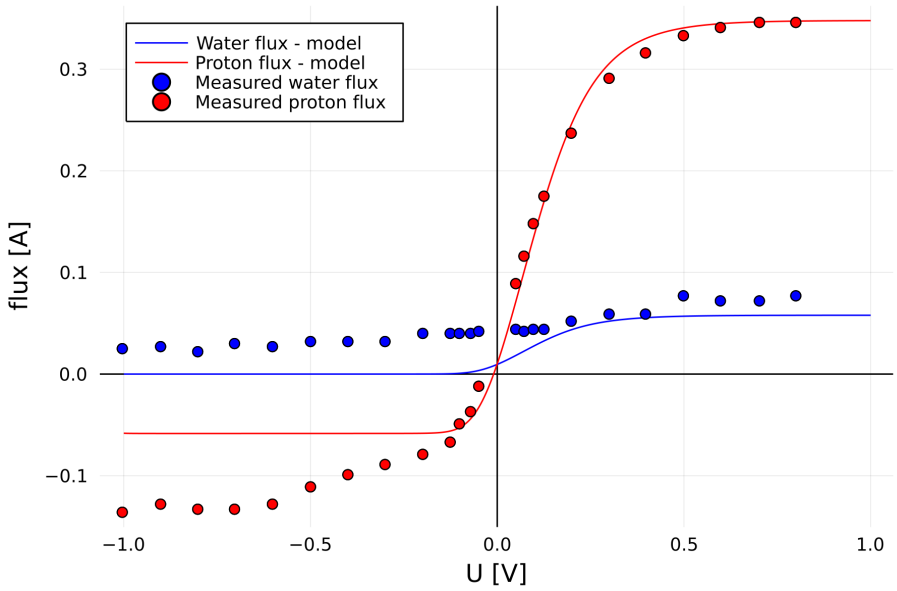

Figure 4.6: The results of the CIT model for boundary conditions $RH|_{left} = 30\%$ and $RH|_{right} = 0\%$ in comparison with the measured data for the same humidity of electrode feeds. Although the proton flux in co-current operation seems to be approximated well, the model values of proton flux are smaller (in absolute value) for counter-current operation.

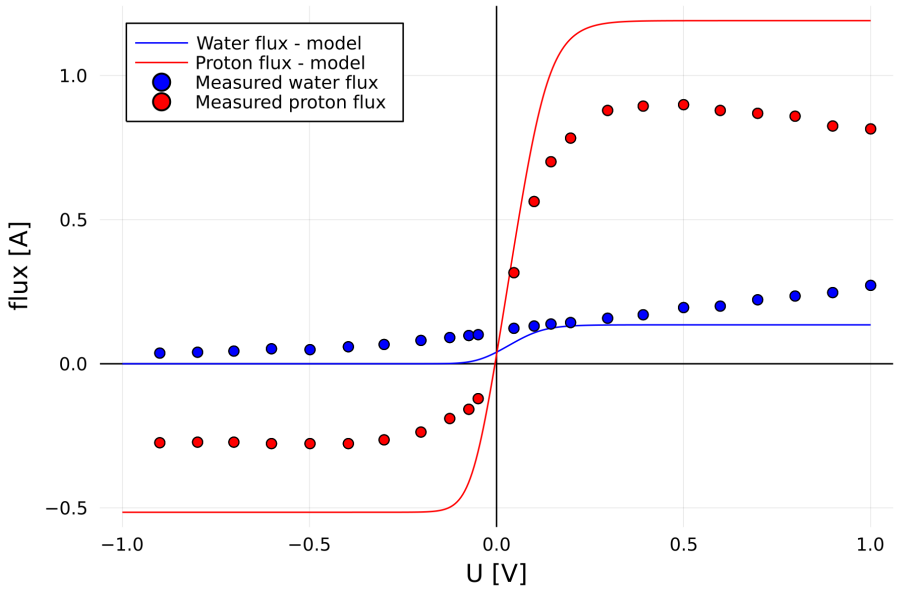

Figure 4.7: The results of the CIT model for boundary conditions $RH|_{left} = 70\%$ and $RH|_{right} = 0\%$ in comparison with the measured data for the same humidity of electrode feeds. The model proton flux for both co-current and counter-current operations is much bigger (in absolute value) than the measured flux.

X_p and j_p. This can be done by expressing X_w from 1.55 as a function of j_p and X_p and plugging it into 1.56. We get

$$j_w = \frac{L_{ww}}{L_{pw}} j_p - \frac{L_{ww}L_{pp}}{L_{pw}} X_p + L_{wp} X_p. \tag{4.2}$$

Taking the derivative with respect to X_p, while keeping j_p constant we get

$$\left(\frac{\partial j_w}{\partial X_p}\right)_{j_p=const.} = -\frac{L_{ww}L_{pp}}{L_{pw}} + L_{wp} \tag{4.3}$$

$$= -\frac{1}{L_{pw}}\left(L_{ww}L_{pp} - L_{wp}L_{pw}\right) \tag{4.4}$$

$$= -\frac{\det \mathbf{L}}{L_{pw}}. \tag{4.5}$$

As the determinant of matrix $\mathbf{L}$ is strictly positive as a consequence of positive entropy production, we get that water flux can grow with increasing the voltage while j_p is kept constant only for $L_{pw} < 0$. That would mean $\xi < 0$, which does not make sense from a physical point of view. Therefore, we can assume that the addition to our model should be made for the equations on the boundary. A more detailed analysis of how the equations could be changed will be provided in the discussion.

4.3 Why drag coefficient can not be directly measured?

The measurements of drag coefficient (defined as 1.63) can be done in multiple ways [23]. One of them is measurement on the hydrogen pump, which proceeds as follows. The relative humidity is set to be the same on both sides. This is done to assure that the thermodynamical force acting on water X_w is zero. Then an electric potential is applied to the membrane, and the water flux and proton flux are measured. The drag coefficient is then given as a water flux and proton flux ratio [24].

However, as we have seen in figure 4.3 the profile of water activity inside the membrane depended strongly on applied potential and was not trivial. Therefore, it is not possible to assume that after setting $RH|_{left} = RH|_{right}$ the water activity will be constant inside the membrane for the non-zero applied voltage. Due to just presented arguments, it is impossible to determine the drag coefficient simply as a ratio of experimentally measured j_w and j_p. To prove that, we ran multiple simulations of hydrogen pump for multiple values of RH, whereas $RH|_{left} = RH|_{right}$ in every simulation. We calculated the ratio of j_w and j_p, which were the simulation results, and plotted them as a function of applied voltage. The simulation results for humidities in the range from 5% to 45% are shown in figure 4.8. As can be seen from the figure, the drag coefficient values decrease linearly as a function of RH on the boundaries (if we neglect the peaks for small voltages). The reason is that the water activity profiles have the same shape for every value of RH (we can denote the shape as $k_{RH} \cdot g(x)$, where k_{RH} is a constant for a specific value of RH), and they differ just by the multiplication constant k_{RH}. Therefore, the X_w, which is proportional to the gradient of water activity, must grow linearly by increasing the value of RH. This observation gives us a simple way how drag coefficient can be extracted from experimental data — it can be taken as an interpolated value of experimentally measured function $\xi_{meas.}(RH|_{boundary})$ for $RH = 0\%$.

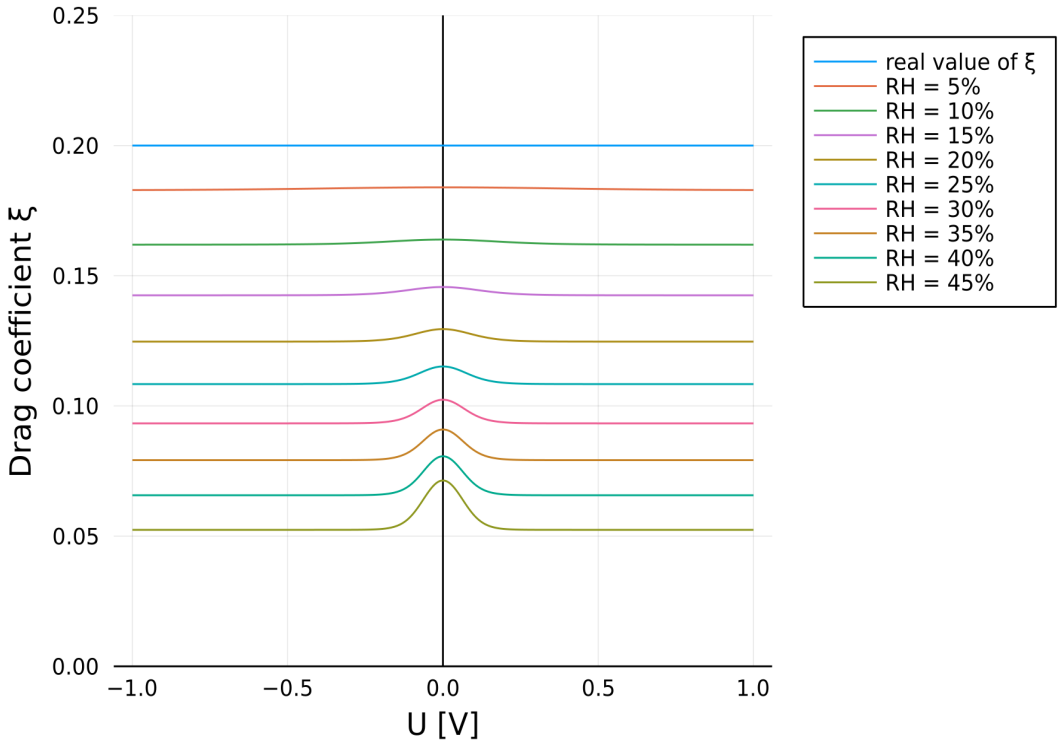

Figure 4.8: The figure shows the simulation results for drag coefficient determined as a ratio if j_w and j_p considering the X_w was set to be zero (from the point of an observer by setting RH to be the same on both sides of the membrane). However, as the proton flux inside the membrane interacts with the water molecules (due to electro-osmotic drag), the water activity profile was not flat inside the membrane, and X_w was non-zero (negative) inside the membrane.

5. Discussion

The main goal of the discussion is to provide the explanation how our model could be extended to have better agreement with measured data. As we have already shown, the extension of model can not be done for equations inside the membrane 4.2 and only boundary equations can be modified.

Therefore, we will recall equations on the boundary. Although we have 4 boundary equations (equation on each side for every species), equations for one species on different sides on the membrane share the common structure, therefore, we will write down only one equation for each species. For the water flux we have

$$j_w = k_w \left(a_w|_{right} - a_w|_{left}\right) \tag{5.1}$$

where $a_w|_{right}$ means the limit of water activity in the boundary point on from the right side and $a_w|_{left}$ means the limit from the left side (as in general the water activity is not continuous on the boundary and water flux is given by the size of this activity jump). For the proton flux we have

$$j_p = j_0 \sinh(\eta_{HOR}) = j_0^{HOR} a_C L_C \sinh(\eta_{HOR}), \tag{5.2}$$

where the η_{HOR} is the overpotential of the HOR reaction proceeding on the electrode.

What can be done to modify the equations is to change the constants k_w and j_0. In general, the j_0 can be rewritten as a product of j_0^{HOR}, a_C and L_C 5.2. The first represents the reaction itself, and the latter two represent the place where the reaction proceeds. L_C represents how much platinum is there (in mg) per cm^2, which is given by the construction of the electrode. j_0^{HOR} is a specific constant for the reaction, and a_C stands for the active surface in cm^2 per mg of platinum where the reaction can proceed. As the hydrogen pump operates, part of the active surface may be blocked due to water flux. That would slow down the reaction. Such dependence could be expressed as $a_C = a_C(j_w)$. Such extension would couple the proton production with the water flux on the boundary. It could also make the proton flux saturation a consequence of lowering the j_p, not a consequence of the dry spot in the membrane.

Therefore, we tried what impact would have introduced a modification to the theory. As we do not have any theoretical background as a base for our model, we assumed that the active surface is decreasing linearly with the water flux. Therefore, the model looks

$$a_C = k_1 - k_2 j_w \tag{5.3}$$

where k_1 and k_2 are some constants. The new model should be fitted with a new set of parameters σ_p^0, k_w, and ξ. However, we will not do it, as we want to see whether such a modification can cause the proton flux saturation without saturation of water flux. Results of a model for the set of parameters σ_p^0, k_w and ξ with values presented in previous chapter and for different values of k_1 are shown in figure 5.1. The value of k_2 was fixed at $k_2 = 1$, because we found out that the result does not depend on both parameters k_1 and k_2 but just on their ratio. As can be seen from the figure 5.1, the greater the k_1, the smaller the influence of water flux on the active surface. For such a case ($k_1 = 50$), the fluxes are almost

identical as in the case where the dependence of a_C on j_w was not assumed (see figure 4.1)

From the figure 5.1 can be, however, seen that even if we assume dependence of a_C on j_w as presented in 5.3 the water flux saturates for the same value of U as the proton flux. That means that introduced simple modification can not resolve our problem, and a more detailed look into how the active surface is affected by water flux is needed. Moreover, there is no guarantee that the humidity on the

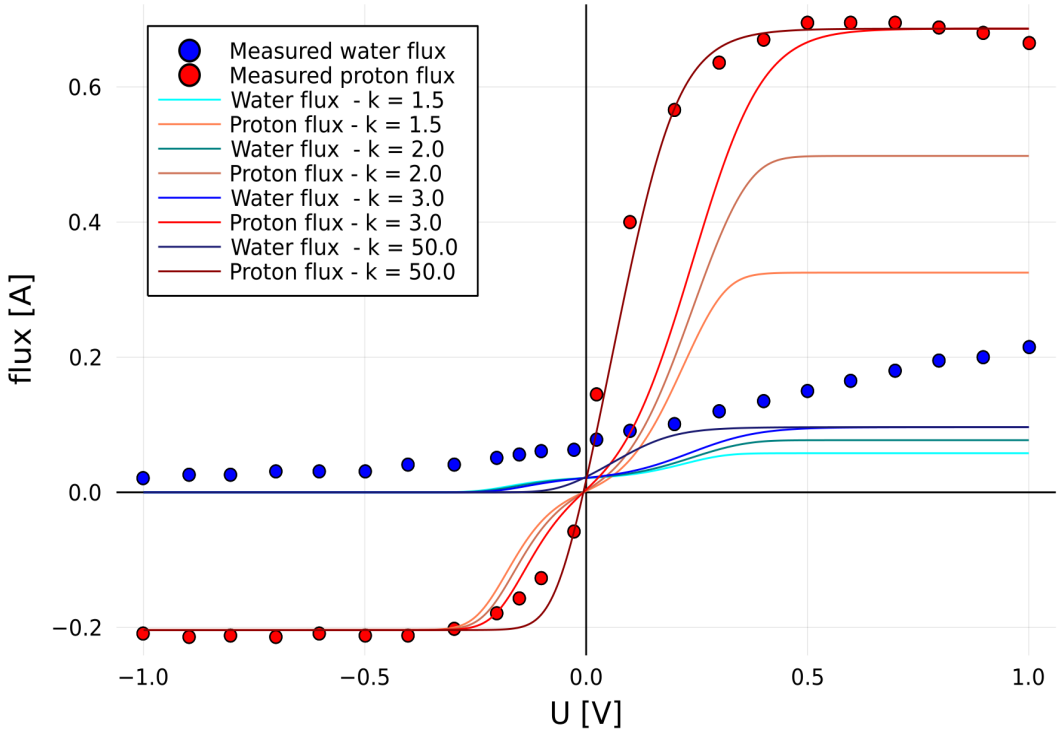

Figure 5.1: The figure shows the model fluxes for different values of parameter k_1. The parameter k_2 was set to be one (as the fluxes appeared to be independent of the values of k_1 and k_2, and depended only on their ratio.) instead of k_1 the legend uses the notation k. It can be seen that although the parameter k has an impact on the shape of the curves, the proton flux saturation occurs at the same time as the saturation of water flux, which means that such a simple modification (5.3) is unable to solve the saturation of water flux.

electrodes is spatially constant in the experimental setup. In our model, we tried to take into account not only the humidity of the electrode feed but also of the effluents. Specifically, we tested the humidity on the electrode to be the weighted averages of humidity of the feed and humidity of the effluent. That, however, gave us results with a much worse agreement with experiments, as in the case where we assumed that the humidity near the electrode is equal to the humidity of the feed. Although the averaging did not work, better results could be achieved with a more complex model. Therefore, developing the two-dimensional or even three-dimensional model could be a promising idea for future research.

The second thing to discuss is to explain why the fitted value of the proton conductivity of the membrane differs so much from the measurements from [17]. The difference was presented in Figure 4.2. As we have mentioned before, the

measurement is done as a measurement of the resistivity for small voltages but using alternating current ([17]). The constant water activity inside the membrane was set during the experiments, and then alternating voltage was applied. However, we can not say what would happen in such a case. Such a system is very far from reaching a stationary state, and therefore, we do not know how the water activity profile would behave. However, we could assume that because drying of the membrane was not considered in previous works, this fact was not taken into account while designing the experiments for conductivity measurement. To conclude whether the problem is in our model or in the experiments, a consultation with the authors of the experiment would be needed.

The last thing that should be discussed is the drag coefficient measurements. Several approaches can be used to measure the drag coefficient, and some of them give different results than the others ranging from 0.1 to 2.9 [23]. Moreover, in all the works, drag is measured as a function of water activity, which is in contradiction with the theoretical results introduced in [13] and again derived under more restrictive but more useful (for our purpose) conditions in the section 1.3.2. As we proposed at the beginning of the section 4.3, the basic condition for the drag measurements (setting $X_w = 0$) is not satisfied by setting $RH|_{left} = RH|_{right}$ as the water activity profile inside the membrane is still non-trivial. We also proposed that the right value of the drag could be obtained by interpolating the measured function $\xi_{meas.}(RH|_{boundary})$ to the point $RH = 0\%$. However, if we interpolate the data (just by the hand) from the [24], we see that their measurements gave three to four times higher values of the drag coefficient. The difference can be caused by the fact that they made the measurement in the following way. On both sides, the constant humidity was set. Then the voltage was applied. After the system reached the stationary state, the water flux was calculated from the humidity change on both sides. However, that means that during the measurement, water concentration was different on both sides, which means that the condition $X_w = 0$ was not even macroscopically satisfied. Due to just presented inconsistency, the comparison with the experiment can not be made, as our model was describing different situation.

Conclusion

The main goal of the thesis was to formulate the one-dimensional CIT model for the experimental setup of the hydrogen pump introduced in [1]. After doing it, we implemented the equations numerically in the VoronoiFVM library in Julia. With such an implementation, we tried to explain the data measured in [1]. More specifically, the flux of protons and water was measured as a function of applied voltage. A saturation of proton flux was observed.

Our model predicted the same proton flux saturation, with some fitted set of constants σ_p^0, ξ, and k_w, as were the experimental data for anode feed with 50% humidity. However, the model failed to predict fluxes for feeds with 30% and 70% humidity. The model also predicted the water flux to saturate at a specific value for the same voltage, where the proton flux saturated. That was in contradiction with the measured data, however, as we have shown, this was the necessary result of our model, as the same mechanism caused the saturation of proton flux and saturation of water flux – drying of the membrane near the anode as a consequence of water molecules being dragged by moving protons. We proposed how this issue could be fixed – if we assumed that the active surface of the electrode, which is the surface where the reaction proceeds, was shrinking due to increasing water flux. That could lead to saturation of proton flux earlier than the dry spot occurs. That would lead to proton flux saturation without saturating the water flux. We tried the model in its simple form, and this modification does not seem to work as we thought – saturation of water flux and proton flux occurred simultaneously. That means a better model for the dependence of active surface on water flux should be made in the future. It also means that the current saturation occurs because of membrane drying and not due to the shrinking of the active surface.

Because our CIT model without the dependence of active surface on water flux gave us an excellent qualitative explanation of what causes a proton flux saturation, we used fitted constants of the model σ_p^0 and ξ to compare them with the experimentally measured values of the proton conductivity of Nafion (as a function of water activity) and the drag coefficient. We found out that the measured proton conductivity presented in [17] as a function of water activity appeared to be one order smaller than the experimentally gained results. The reason could be that the water activity inside a membrane was considered constant during the measurements. In other words, conductivity was considered to be just one number for the membrane for specific feed humidity, which we know can lead to wrong results. On the other hand, conductivity was obtained from AC resistance measurement, which means that the whole system was very far from a stationary state (due to the fast changing of applied potential), and our model can not predict how the system behaves in such a state. Therefore, we can not answer whether the used measurements techniques were right. As the author of the experiments did not discuss water activity profile change inside the membrane and membrane drying, it would be needed to consult with him about our results to say whether the measurement method is problematic or whether the model gives bad results.

The drag coefficient ξ is experimentally measured always as a function of water activity in the membrane. However, as we have shown in 1.3.2, the drag

coefficient must be constant. We used our model to simulate the measurements of the drag coefficient, and indeed we found the dependence on the water activity of the gas surrounding the membrane. We also found out and later explained that the real value of the drag coefficient can be obtained from interpolation of the drag measurement as a function of a_w to the point where $a_w = 0$.

A. Finite volume method

The finite volume method is based on discretisation of the domain into the small volumes and then integration of equations over the volumes. The integrals are then approximated numerically. This method takes advantage of this construction when dealing with terms in shape of the $\nabla \cdot \mathbf{j}$, because Gauss theorem can be used to get rid of this terms ([25]). In the next section we will demonstrate the method on the 1D example for diffusion equation with a constant source term and Dirichlet boundary condition on the left hand side and Neumann boundary condition on the right hand side.

A.1 Finite volumes for 1D diffusion

The formulation of our problem is

$$\nabla \cdot j_\phi = d_x^2 \phi = f(x) = 2 \qquad x \in (0,1) \tag{A.1}$$

$$\phi = 1 \qquad x = 0 \tag{A.2}$$

$$d_x \phi = 1 \qquad x = 1, \tag{A.3}$$

which has analytical solution in the form

$$\phi(x) = x^2 - x + 1. \tag{A.4}$$

Further we will assume the discrete version of function $\phi(x)$, which will be a constant on each control volume and will be denoted $\varphi(x)$.

Now we have to define the grid, where A.1 will be solved numerically. The grid consists at first of nodes (which lies inside of each piece of the domain, called *control volume*. The exceptions are boundary nodes, which lies on the boundary of the domain and therefore on the boundary of the respective control volumes). As we have mentioned we consider every function to be constant in every control volume. Its value inside the certain volume will be represented by the value of the function in the respective node. Except of nodes and control volumes, the grid contains boundaries of the volumes called *faces* (For one dimensional problem faces are points, but generally faces are objects with dimension one less than the dimension of the problem). If we have two neighbouring volumes A and B, with respective nodes a and b, they are separated with the face f_{AB}. [1]

We will proceed by integrating the equation A.1 where the solution ϕ is replaced with the discrete version of the solution $\varphi(x)$ over the control volume B

$$\int_B \nabla \cdot j_\varphi dx - \int_B f(x) dx = 0 \tag{A.5}$$

$$\int_B d_x j_\varphi dx - 2 \int_B dx = 0 \tag{A.6}$$

$$j_\varphi(f_{BC}) - j_\varphi(f_{AB}) - 2\,|B| = 0, \tag{A.7}$$

[1] Note that nodes do not necessary have to be placed in the centre of respective control volume. This happens if neighbouring control volumes do do not have the same volume. See picture A.1, specifically node d

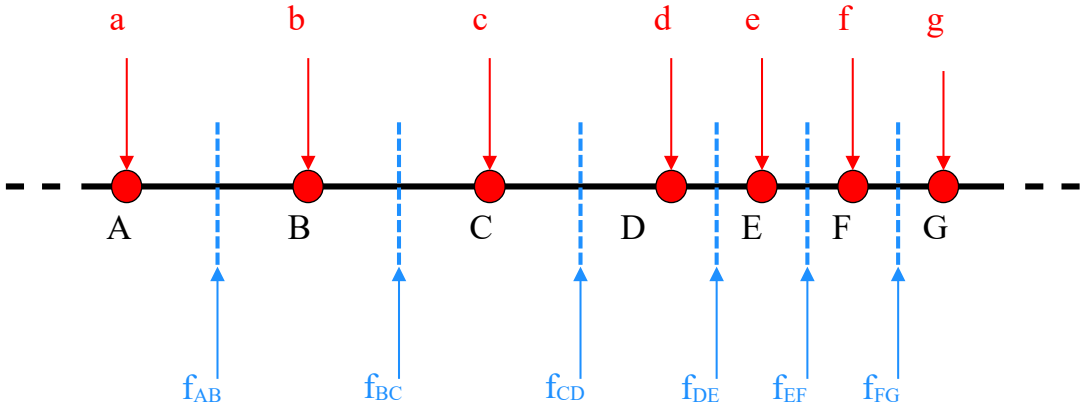

Figure A.1: The picture shows the sketch of one dimensional grid. Nodes (red circles, denoted with small letters) are selected to cover the domain in the way, that regions where the solution is expected to change more dramatically should have higher density of nodes. The point in the middle between two nodes is the boundary between two control volumes (denoted with capital letters), which is called *face* and denoted as f with subscript which corresponds to the names of neighbouring control volumes (for example boundary between control volume C – which contains node c, and control volume D – which contains node d is called f_{CD}). This construction causes, that the node do not have to be in the centre of control volume, as can be seen on node D, which is shifted in the direction to face f_{DE} as nodes are more dense from D to the right.

where in A.6 we used the fact that ∇ operator in 1D is simply spatial derivative and therefore from A.1 flux j_φ is equal to the derivative of φ (In general the flux can be more complicated). To proceed to expression A.7 we used the notation of faces of control volume B introduced on picture A.1 and where $|B|$ denotes the size of control volume B. As $\varphi(x)$ is defined to be a constant inside each control volume, we need to approximate its flux on the face somehow. The most convenient way is simply

$$j_\varphi(f_{BC}) \approx \frac{\varphi(c) - \varphi(b)}{c - b} \tag{A.8}$$

$$j_\varphi(f_{AB}) \approx \frac{\varphi(b) - \varphi(a)}{b - a}, \tag{A.9}$$

where a, b and c are simply the x coordinates of respective points. After pluging A.8 and A.9 into A.7. we get

$$\frac{\varphi(c) - \varphi(b)}{c - b} - \frac{\varphi(b) - \varphi(a)}{b - a} - 2\,|B| = 0, \tag{A.10}$$

which is an equation for three unknowns $\varphi(c)$, $\varphi(b)$ and $\varphi(a)$ with some coefficients which depends on the grid (a, b, c and $|B|$) and another which depends on another

given terms (in this case there is only one additional term – source term, and is given by the number 2). If we would write down the equation for control volume C, we will again get similar equation, but with variables $\varphi(b)$, $\varphi(c)$ and $\varphi(d)$, which adds us one additional unknown. This gives us $n + 2$ unknowns for the system of n equations. To have the unique solution, we need another two equations, which are given by boundary conditions. For Dirichlet boundary condition A.2 we can simply write $\varphi(0) = 1$. For Neumann boundary condition we can assume for instance, that the prescribed derivative on the boundary, is prescribed for the derivative on face between $(n-1)$-th and n-th control volumes. If we denote them U and V respectively it holds

$$d_x\phi = 1 \implies \frac{\varphi(v) - \varphi(u)}{v - u} = 1. \tag{A.11}$$

Now we have n linear equations for n nodes, so if system of equations A.1, A.2 and A.3 was well posed, derived system on linear equations will have unique solution.

Bibliography

[1] Jay Benziger, May Cheah, Václav Klika, and Michal Pavelka. Interfacial constraints on water and proton transport across nafion membranes. *Journal of Polymer Science Part B: Polymer Physics*, 53, 08 2015.

[2] Shahriar Shafiee and Erkan Topal. When will fossil fuel reserves be diminished? *Energy Policy*, 37(1):181–189, 2009.

[3] Jeff Tollefson. How hot will earth get by 2100? *Nature*, 580:443–445, 04 2020.

[4] Norazlianie Sazali, Wan Norharyati, Ahmad Jamaludin, and Mohd Razali. New perspectives on fuel cell technology: A brief review. *Membranes*, 10:99, 05 2020.

[5] Francesco Baldi, Ligang Wang, Mar Pérez-Fortes, and François Maréchal. A cogeneration system based on solid oxide and proton exchange membrane fuel cells with hybrid storage for off-grid applications. *Frontiers in Energy Research*, 6, 2019.

[6] Kannihalli Bhaskar, Jenoris Muthiya, Ravishankar Sathyamurthy, V. Shridhar, and Nadana Vinayagam. A review on pem fuel cells used for automotive applications, models and hydrogen storage for hybrid electric fuel cell vehicle. 12 2020.

[7] V. Matolín, M. Cabala, I. Matolínová, M. Škoda, M. Václavů, K.C. Prince, T. Skála, T. Mori, H. Yoshikawa, Y. Yamashita, S. Ueda, and K. Kobayashi. Pt and sn doped sputtered ceo2 electrodes for fuel cell applications. *Fuel Cells*, 10(1):139–144, 2010.

[8] Benziger group. `http://pemfc.princeton.edu/PEMFC_members.html`. Accessed: 2022-04-25.

[9] S.R. de Groot, S.R. Groot, and P. Mazur. *Non-equilibrium Thermodynamics*. Dover books on physics and chemistry. North-Holland Publishing Company, 1962.

[10] Georgy Lebon, David Jou, and Casas-Vázquez José. *Understanding Non-Equilibrium Thermodynamics*. 01 2008.

[11] Michal Pavelka. *Thermodynamic analysis of processes in hydrogen fuel cells*. PhD thesis, 06 2015.

[12] First edition. edition, 2008.

[13] Václav Klika, Michal Pavelka, and Jay Benziger. Functional constraints on phenomenological coefficients. *Physical Review E*, 95, 01 2017.

[14] P. W. (Peter William) Atkins. *Atkins' Physical chemistry*. Oxford University Press, Oxford, United Kingdom ;, eleventh edition. edition, 2018.

[15] Václav Klika, Jan Kubant, Michal Pavelka, and Jay Benziger. Non-equilibrium thermodynamic model of water sorption in nafion membranes. *Journal of Membrane Science*, 540, 06 2017.

[16] Frano Barbir. *PEM fuel cells theory and practice / Frano Barbir.* Elsevier/Academic Press, Amsterdam ; Boston, 2nd ed. edition, 2013.

[17] Jay Benziger, Andrew Bocarsly, May Cheah, Paul Majsztrik, Barclay Satterfield, and Qiao Zhao. *Mechanical and Transport Properties of Nafion: Effects of Temperature and Water Activity*, volume 141, pages 85–113. 04 2011.

[18] Kei Morohoshi and Takahiro Hayashi. Modeling and simulation for fuel cell polymer electrolyte membrane. *Polymers*, 5:56–76, 03 2013.

[19] Kenneth Mauritz and Robert Moore. State of understanding of nafion. *Chemical reviews*, 104:4535–85, 12 2004.

[20] Hui Li, Chaojie Song, and Jianlu Zhang. *Catalyst Contamination in PEM fuel cells.* 01 2008.

[21] J. Fuhrmann and contributors. VoronoiFVM.jl: Finite volume solver for coupled nonlinear partial differential equations.

[22] Pyoungho Choi, Nikhil Jalani, and Ravindra Datta. Thermodynamics and proton transport in nafion ii. proton diffusion mechanisms and conductivity. *Journal of The Electrochemical Society*, 152:E123–E130, 03 2005.

[23] Feina Xu, Sebastien Leclerc, Didier Stemmelen, Jean-Christophe Perrin, Alain Retournard, and Daniel Canet. Study of electro-osmotic drag coefficients in nafion membrane in acid, sodium and potassium forms by electrophoresis nmr. *Journal of Membrane Science*, 536, 05 2017.

[24] Zhe Peng, Arnaud Morin, Patrice Huguet, Pascal Schott, and Joël Pauchet. In-situ measurement of electroosmotic drag coefficient in nafion membrane for the pemfc. *The journal of physical chemistry. B*, 115:12835–44, 09 2011.

[25] Henk Kaarle Versteeg and Weeratunge Malalasekera. *An introduction to computational fluid dynamics - the finite volume method.* Addison-Wesley-Longman, 1995.

List of Abbreviations

FVM	Finite Volume Method
PEM	Proton Exchange Membrane
HOR	Hydrogen Oxidation Reaction
CIT	Classical Irreversible Thermodynamics
O-C	Onsager-Casimir's (relations)
OCRR	Onsager-Casimir Reciprocal Relations
HRR	Hydrogen Reduction Reaction
RH	Relative Humidity
ODE	Ordinary Differential Equation
OCV	Open Circuit Voltage
FC	Fuel Cell
EW	Equivalent Weight